Modeling of a Diesel Engine with VGT and EGR capturing Sign Reversal and Non-minimum Phase Behaviors

Johan Wahlström and Lars Eriksson

Vehicular systems
Department of Electrical Engineering
Linköpings universitet, SE-581 83 Linköping, Sweden
WWW: www.vehicular.isy.liu.se
E-mail: {johwa, larer}@isy.liu.se
Report: LiTH-ISY-R-2882

March 23, 2009

When citing this work, it is recommended that the citation is the improved and extended work, published in the peer-reviewed article Johan Wahlström and Lars Eriksson, Modeling diesel engines with a variable-geometry turbocharger and exhaust gas recirculation by optimization of model parameters for capturing non-linear system dynamics, Proceedings of the Institution of Mechanical Engineers, Part D, Journal of Automobile Engineering, Volume 225, Issue 7, July 2011, http://dx.doi.org/10.1177/0954407011398177.

Abstract

A mean value model of a diesel engine with VGT and EGR is developed and validated. The intended model applications are system analysis, simulation, and development of model-based control systems. The goal is to construct a model that describes the dynamics in the manifold pressures, turbocharger, EGR, and actuators with few states in order to have short simulation times. Therefore the model has only eight states: intake and exhaust manifold pressures, oxygen mass fraction in the intake and exhaust manifold, turbocharger speed, and three states describing the actuator dynamics. The model is more complex than e.g. the third order model in [12] that only describes the pressure and turbocharger dynamics, but it is considerably less complex than a GT-POWER model or a Ricardo WAVE model. Many models in the literature, that approximately have the same complexity as the model proposed here, use three states for each control volume in order to describe the temperature dynamics. However, the model proposed here uses only two states for each manifold. Model extensions are investigated showing that inclusion of temperature states and pressure drop over the intercooler only have minor effects on the dynamic behavior and does not improve the model quality. Therefore, these extensions are not included in the proposed model. Model equations and tuning methods are described for each subsystem in the model. In order to have a low number of tuning parameters, flows and efficiencies are modeled using physical relationships and parametric models instead of look-up tables. To tune and validate the model, stationary and dynamic measurements have been performed in an engine laboratory at Scania CV AB. Static and dynamic validations of the entire model using dynamic experimental data show that the mean relative errors are 12.7 % or lower for all measured variables. The validations also show that the proposed model captures the essential system properties, i.e. a non-minimum phase behavior in the channel u_{egr} to p_{im} and a non-minimum phase behavior, an overshoot, and a sign reversal in the channel u_{vgt} to W_c.

Contents

1 Introduction

Legislated emission limits for heavy duty trucks are constantly reduced. To fulfill the requirements, technologies like Exhaust Gas Recirculation (EGR) systems and Variable Geometry Turbochargers (VGT) have been introduced. The primary emission reduction mechanisms utilized to control the emissions are that NO_x can be reduced by increasing the intake manifold EGR-fraction x_{egr} and smoke can be reduced by increasing the oxygen/fuel ratio λ_O [11]. However x_{egr} and λ_O depend in complicated ways on the actuation of the EGR and VGT. It is therefore necessary to have coordinated control of the EGR and VGT to reach the legislated emission limits in NO_x and smoke. When developing and validating a controller for this system, it is desirable to have a model that describes the system dynamics and the nonlinear effects that are important for gas flow control. For example in [14], [13], and [19] it is shown that this system has non-minimum phase behaviors, overshoots, and sign reversals. Therefore, the objective of this report is to construct a mean value diesel engine model, from actuator input to system output, that captures these properties. The intended usage of the model are system analysis, simulation and development of model-based control systems. The model shall describe the dynamics in the manifold pressures, turbocharger, EGR, and actuators with few states in order to have short simulation times.

Several models with different selections of states and complexity have been published for diesel engines with EGR and VGT. A third order model that describes the intake and exhaust manifold pressure and turbocharger dynamics is developed in [12]. The model in [13] has 6 states describing intake and exhaust manifold pressure and temperature dynamics, and turbocharger and compressor mass flow dynamics. A 7:th order model that describes intake and exhaust manifold pressure, temperature, and air-mass fraction dynamics, and turbocharger dynamics is proposed in [1]. These dynamics are also described by the 7:th order models in [12, 14, 19] where burned gas fraction is used instead of air-mass fraction in the manifolds. Another model that describes these dynamics is the 9:th order model in [18] that also has two states for the actuator dynamics. The models described above are lumped parameter models. Other model families, that have considerably more states are those based on one-dimensional gas dynamics, for example GT-POWER and Ricardo WAVE models.

The model proposed here has eight states: intake and exhaust manifold pressures, oxygen mass fraction in the intake and exhaust manifold, turbocharger speed, and three states describing the actuator dynamics. In order to have a low number of tuning parameters, flows and efficiencies are modeled based upon physical relationships and parametric models instead of look-up tables. The model is implemented in MATLAB/SIMULINK using a component library.

1.1 Outline and model extensions

The structure of the model as well as the tuning and the validation data are described in Sec. 1.2 to 1.6. Model equations and model tuning are described for each sub-model in Sec. 2 to 6. A summary of the model assumptions and the model equations is given in Sec. 7 while Sec. 8 summarizes the tuning and a model validation. The goal is also to investigate if the proposed model can be

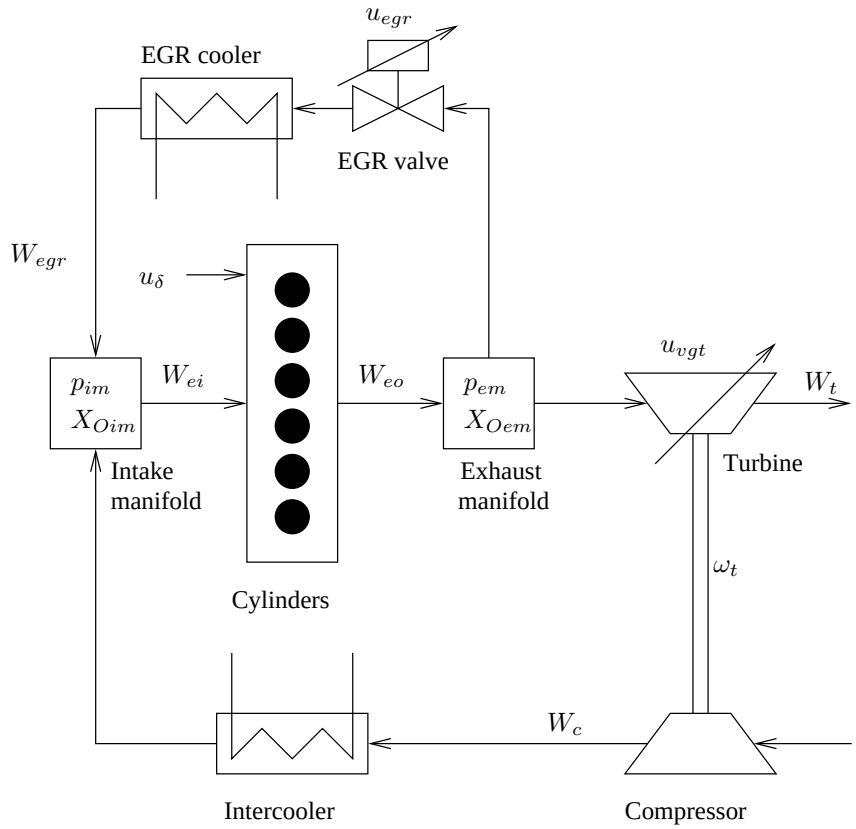

Figure 1: A model structure of the diesel engine. It has three control inputs and five main states related to the engine (p_{im}, p_{em}, X_{Oim}, X_{Oem}, and ω_t). In addition, there are three states for actuator dynamics ($\tilde{u}_{egr1}$, $\tilde{u}_{egr2}$, and $\tilde{u}_{vgt}$).

improved with model extensions in Sec. 9. These model extensions are inclusions of temperature states and a pressure drop over the intercooler and they are investigated due to that they are used in many models in the literature [2, 8, 12, 14, 18].

1.2 Selection of number of states

The model has eight states: intake and exhaust manifold pressures (p_{im} and p_{em}), oxygen mass fraction in the intake and exhaust manifold (X_{Oim} and X_{Oem}), turbocharger speed (ω_t), and three states describing the actuator dynamics for the two control signals ($\tilde{u}_{egr1}$, $\tilde{u}_{egr2}$, and $\tilde{u}_{vgt}$). These states are collected in a state vector x

$$x = (p_{im} \quad p_{em} \quad X_{Oim} \quad X_{Oem} \quad \omega_t \quad \tilde{u}_{egr1} \quad \tilde{u}_{egr2} \quad \tilde{u}_{vgt})^T \tag{1}$$

Descriptions of the nomenclature, the variables and the indices can be found in Appendix A and the structure of the model can be seen in Fig. 1.

The states p_{im}, p_{em}, and ω_t describe the main dynamics and the most important system properties, such as non-minimum phase behaviors, overshoots,

and sign reversals. In order to model the dynamics in the oxygen/fuel ratio λ_O, the states X_{Oim} and X_{Oem} are used. Finally, the states $\tilde{u}_{egr1}$, $\tilde{u}_{egr2}$, and $\tilde{u}_{vgt}$ describe the actuator dynamics where the EGR-valve actuator model has two states ($\tilde{u}_{egr1}$ and $\tilde{u}_{egr2}$) in order to describe an overshoot in the actuator.

Many models in the literature, that approximately have the same complexity as the model proposed here, use three states for each control volume in order to describe the temperature dynamics [12, 14, 18]. However, the model proposed here uses only two states for each manifold: pressure and oxygen mass fraction. Model extensions are investigated in Sec. 9.1 showing that inclusion of temperature states has only minor effects on the dynamic behavior. Furthermore, the pressure drop over the intercooler is not modeled since this pressure drop has only small effects on the dynamic behavior. However, this pressure drop has large effects on the stationary values, but these effects do not improve the complete engine model, see Sec. 9.2.

1.3 Model structure

It is important that the model can be utilized both for different vehicles and for engine testing and calibration. In these situations the engine operation is defined by the rotational speed n_e, for example given as an input from a drivecycle, and therefore it is natural to parameterize the model using engine speed. The resulting model is thus expressed in state space form as

$$\dot{x} = f(x, u, n_e) \tag{2}$$

where the engine speed n_e is considered to be an input to the model, and u is the control input vector

$$u = (u_\delta \quad u_{egr} \quad u_{vgt})^T \tag{3}$$

which contains mass of injected fuel u_δ, EGR-valve position u_{egr}, and VGT actuator position u_{vgt}. The EGR-valve is closed when $u_{egr} = 0\,\%$ and open when $u_{egr} = 100\,\%$. The VGT is closed when $u_{vgt} = 0\,\%$ and open when $u_{vgt} = 100\,\%$.

1.4 Measurements

To tune and validate the model, stationary and dynamic measurements have been performed in an engine laboratory at Scania CV AB, and these are described below.

1.4.1 Stationary measurements

The stationary data consists of measurements at stationary conditions in 82 operating points, that are scattered over a large operating region covering different loads, speeds, VGT- and EGR-positions. These 82 operating points also include the European Stationary Cycle (ESC) at 13 operating points. The variables that were measured during stationary measurements can be seen in Tab. 1. The EGR fraction is calculated by measuring the carbon dioxide concentration in the intake and exhaust manifolds.

All the stationary measurements are used for tuning of parameters in static models. The static models are then validated using dynamic measurements.

Table 1: Measured variables during stationary measurements.

Variable	Description	Unit
M_e	Engine torque	Nm
n_e	Rotational engine speed	rpm
n_t	Rotational turbine speed	rpm
p_{amb}	Ambient pressure	Pa
p_c	Pressure after compressor	Pa
p_{em}	Exhaust manifold pressure	Pa
p_{im}	Intake manifold pressure	Pa
T_{amb}	Ambient temperature	K
T_c	Temperature after compressor	K
T_{em}	Exhaust manifold temperature	K
T_{im}	Intake manifold temperature	K
T_t	Temperature after turbine	K
u_{egr}	EGR control signal. 0 - closed, 100 - open	%
u_{vgt}	VGT control signal. 0 - closed, 100 - open	%
u_δ	Injected amount of fuel	$mg/cycle$
W_c	Compressor mass flow	kg/s
x_{egr}	EGR fraction	$-$

1.4.2 Dynamic measurements

The dynamic data consists of measurements at dynamic conditions with steps in VGT control signal, EGR control signal, and fuel injection in several different operating points according to Tab. 2. The steps in VGT-position and EGR-valve are performed in 9 different operating points (data sets A-H, J) and the steps in fuel injection are performed in one operating point (data set I). The data set J is used for tuning of dynamic actuator models and the data sets E and I are used for tuning of dynamic models in the manifolds, in the turbocharger, and in the engine torque. Further, the data sets A-D and F-I are used for validation of essential system properties and time constants and the data sets A-I are used for validation of static models. The dynamic measurements are limited in sample rate with a sample frequency of 1 Hz for the data sets A, D-G, 10 Hz for the data set I, and 100 Hz for the data sets B, C, H, and J. This leads to that the data sets A, D-G, and I do not capture the fastest dynamics in the system, while the data sets B, C, H, and J do. Further, the data sets B, C, H, and J were measured 3.5 years after the data sets A, D, E, F, G, I and the stationary data. The variables that were measured during dynamic measurements can be seen in Tab. 3.

1.4.3 Sensor time constants and system dynamics

To justify that the model captures the system dynamics and not the sensor dynamics, the dynamics of the sensors are analyzed and compared with the dynamics seen in the measurements. The time constants of the sensors for the measured outputs during dynamic measurements are shown in Tab. 3. These time constants are based on sensor data sheets, except for the time constant for the engine torque sensor that is calculated from dynamic measurements according to Sec. 8.1. The time constants of the sensors for n_t, p_{em}, p_{im},

Table 2: Dynamic tuning and validation data that consist of steps in VGT-position, EGR-valve, and fuel injection. The data sets E, I, and J are used for tuning of dynamic models, the data sets A-D and F-I are used for validation of essential system properties and time constants, and the data sets A-I are used for validation of static models.

	VGT-EGR steps								u_δ steps	VGT-EGR steps
Data set	A	B	C	D	E	F	G	H	I	J
Speed [rpm]	1200				1500	1900			1500	-
Load [%]	25	40	50	75	50	25	75	100	-	-
Number of steps	77	35	2	77	77	77	55	1	7	48
Sample frequency [Hz]	1	100	100	1	1	1	1	100	10	100

Table 3: Measured variables during dynamic measurements and sensor time constants.

Variable	Description	Unit	Maximum time constant for the sensor dynamics [ms]
n_t	Rotational turbine speed	rpm	6
p_{em}	Exhaust manifold pressure	Pa	20
p_{im}	Intake manifold pressure	Pa	15
W_c	Compressor mass flow	kg/s	20
$\tilde{u}_{egr}$	EGR position 0 - closed, 100 - open	%	$\ll 50$
$\tilde{u}_{vgt}$	VGT position 0 - closed, 100 - open	%	$\ll 25$
M_e	Engine torque	Nm	1000
n_e	Rotational engine speed	rpm	26
u_{egr}	EGR control signal 0 - closed, 100 - open	%	-
u_{vgt}	VGT control signal 0 - closed, 100 - open	%	-
u_δ	Injected amount of fuel	$mg/cycle$	-

and W_c are significantly faster than the dynamics seen in the measurements in Fig. 20–22 and these sensor dynamics are therefore neglected. The time constants for the EGR and VGT position sensors are significantly faster than the actuator dynamics and these sensor dynamics are therefore neglected. The time constant for the engine torque sensor is large and it is therefore considered in the validation. However, this time constant is not considered in the proposed model due to that the model will be used for gas flow control and not for engine torque feedback control. Finally, the sensor dynamics for the engine speed does not effect the dynamic validation results since the engine speed is an input to the model and it is also constant in all measurements used here.

1.5 Parameter estimation and validation

Parameters in static models are estimated automatically using least squares optimization and data from stationary measurements. The parameters in the dynamic models are estimated in two steps. Firstly, the actuator parameters are estimated by adjusting these parameters manually until simulations of the actuator models follow the dynamic responses in data set J. Secondly, the manifold volumes, the turbocharger inertia, and the time constant for the engine torque are estimated by adjusting these parameters manually until simulations of the complete model follow the dynamic responses in the data sets E and I.

Systematic tuning methods for each parameter are described in detail in Sec. 2 to 5. Since these methods are systematic and general, it is straightforward to re-create the values of the model parameters and to apply the tuning methods on different diesel engines with EGR and VGT.

Due to that the stationary measurements are few, both the static and the dynamic models are validated by simulating the complete model and comparing it with dynamic measurements. The model is validated in stationary points using the data sets A-I and dynamic properties are validated using the data sets A-D and F-I.

1.6 Relative error

Relative errors are calculated and used to evaluate the tuning and the validation of the model. Relative errors for stationary measurements between a measured variable $y_{meas,stat}$ and a modeled variable $y_{mod,stat}$ are calculated as

$$\text{stationary relative error}(i) = \frac{y_{meas,stat}(i) - y_{mod,stat}(i)}{\frac{1}{N}\sum_{i=1}^{N} y_{meas,stat}(i)} \tag{4}$$

where i is an operating point. Relative errors for dynamic measurements between a measured variable $y_{meas,dyn}$ and a modeled variable $y_{mod,dyn}$ are calculated as

$$\text{dynamic relative error}(j) = \frac{y_{meas,dyn}(j) - y_{mod,dyn}(j)}{\frac{1}{N}\sum_{i=1}^{N} y_{meas,stat}(i)} \tag{5}$$

where j is a time sample. In order to make a fair comparison between these relative errors, both the stationary and the dynamic relative error have the same stationary measurement in the denominator and the mean value of this stationary measurement is calculated in order to avoid large relative errors when $y_{meas,stat}$ is small.

2 Manifolds

The intake and exhaust manifolds are modeled as dynamic systems with two states each, and these are pressure and oxygen mass fraction. The standard isothermal model [11], that is based upon mass conservation, the ideal gas law, and that the manifold temperature is constant or varies slowly, gives the differential equations for the manifold pressures

$$\begin{aligned} \frac{d}{dt} p_{im} &= \frac{R_a T_{im}}{V_{im}} (W_c + W_{egr} - W_{ei}) \\ \frac{d}{dt} p_{em} &= \frac{R_e T_{em}}{V_{em}} (W_{eo} - W_t - W_{egr}) \end{aligned} \tag{6}$$

There are two sets of thermodynamic properties: air has the ideal gas constant R_a and the specific heat capacity ratio γ_a, and exhaust gas has the ideal gas constant R_e and the specific heat capacity ratio γ_e. The intake manifold temperature T_{im} is assumed to be constant and equal to the cooling temperature in the intercooler, the exhaust manifold temperature T_{em} will be described in Sec. 3.2, and V_{im} and V_{em} are the manifold volumes. The mass flows W_c, W_{egr}, W_{ei}, W_{eo}, and W_t will be described in Sec. 3 to 5.

The EGR fraction in the intake manifold is calculated as

$$x_{egr} = \frac{W_{egr}}{W_c + W_{egr}} \tag{7}$$

Note that the EGR gas also contains oxygen that affects the oxygen fuel ratio in the cylinder. This effect is considered by modeling the oxygen concentrations X_{Oim} and X_{Oem} in the control volumes. These concentrations are defined in the same way as in [19]

$$X_{Oim} = \frac{m_{Oim}}{m_{totim}}, \quad X_{Oem} = \frac{m_{Oem}}{m_{totem}} \tag{8}$$

where m_{Oim} and m_{Oem} are the oxygen masses, and m_{totim} and m_{totem} are the total masses in the intake and exhaust manifolds. Differentiating X_{Oim} and X_{Oem} and using mass conservation [19] give the following differential equations

$$\begin{aligned} \frac{d}{dt} X_{Oim} &= \frac{R_a T_{im}}{p_{im} V_{im}} ((X_{Oem} - X_{Oim}) W_{egr} + (X_{Oc} - X_{Oim}) W_c) \\ \frac{d}{dt} X_{Oem} &= \frac{R_e T_{em}}{p_{em} V_{em}} (X_{Oe} - X_{Oem}) W_{eo} \end{aligned} \tag{9}$$

where X_{Oc} is the constant oxygen concentration passing the compressor, i.e. air with $X_{Oc} = 23.14\%$, and X_{Oe} is the oxygen concentration in the exhaust gases coming from the engine cylinders, X_{Oe} will be described in Sec. 3.1.

Another way to consider the oxygen in the EGR gas, is to model the burned gas ratios in the control volumes which are a frequent choice for states in many papers [12, 14, 18]. The oxygen concentration and the burned gas ratio have exactly the same effect on the oxygen fuel ratio and therefore these states are equivalent.

Tuning parameters

- V_{im} and V_{em}: manifold volumes.

Tuning method

The tuning parameters V_{im} and V_{em} are determined by adjusting these parameters manually until simulations of the complete model follow the dynamic responses in the dynamic data set E in Tab. 2.

3 Cylinder

Three sub-models describe the behavior of the cylinder, these are:

- A mass flow model that describes the gas and fuel flows that enter and leave the cylinder, the oxygen to fuel ratio, and the oxygen concentration out from the cylinder.
- A model of the exhaust manifold temperature
- An engine torque model.

3.1 Cylinder flow

The total mass flow W_{ei} from the intake manifold into the cylinders is modeled using the volumetric efficiency η_{vol} [11]

$$W_{ei} = \frac{\eta_{vol}\, p_{im}\, n_e\, V_d}{120\, R_a\, T_{im}} \tag{10}$$

where p_{im} and T_{im} are the pressure and temperature in the intake manifold, n_e is the engine speed and V_d is the displaced volume. The volumetric efficiency is in its turn modeled as

$$\eta_{vol} = c_{vol1}\sqrt{p_{im}} + c_{vol2}\sqrt{n_e} + c_{vol3} \tag{11}$$

The fuel mass flow W_f into the cylinders is controlled by u_δ, which gives the injected mass of fuel in mg per cycle and cylinder

$$W_f = \frac{10^{-6}}{120}\, u_\delta\, n_e\, n_{cyl} \tag{12}$$

where n_{cyl} is the number of cylinders. The mass flow W_{eo} out from the cylinder is given by the mass balance as

$$W_{eo} = W_f + W_{ei} \tag{13}$$

The oxygen to fuel ratio λ_O in the cylinder is defined as

$$\lambda_O = \frac{W_{ei}\, X_{Oim}}{W_f\, (O/F)_s} \tag{14}$$

where $(O/F)_s$ is the stoichiometric relation between the oxygen and fuel masses. The oxygen to fuel ratio is equivalent to the air fuel ratio which is a common choice of performance variable in the literature [12, 15, 16, 18].

During the combustion, the oxygen is burned in the presence of fuel. In diesel engines $\lambda_O > 1$ to avoid smoke. Therefore, it is assumed that $\lambda_O > 1$ and the oxygen concentration out from the cylinder can then be calculated as the unburned oxygen fraction

$$X_{Oe} = \frac{W_{ei}\, X_{Oim} - W_f\, (O/F)_s}{W_{eo}} \tag{15}$$

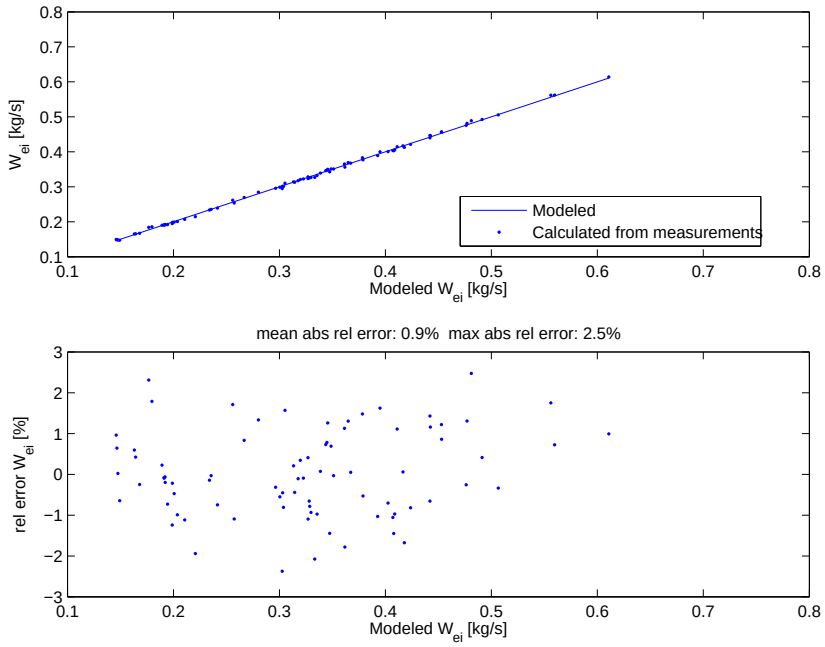

Figure 2: **Top:** Comparison of modeled mass flow W_{ei} into the cylinders and calculated W_{ei} from measurements. **Bottom:** Relative errors for modeled W_{ei} as function of modeled W_{ei} at steady state.

Tuning parameters

- c_{vol1}, c_{vol2}, c_{vol3}: volumetric efficiency constants

Tuning method

The tuning parameters c_{vol1}, c_{vol2}, and c_{vol3} are determined by solving a linear least-squares problem that minimizes $(W_{ei} - W_{ei,meas})^2$ with c_{vol1}, c_{vol2}, and c_{vol3} as the optimization variables. The variable W_{ei} is the model in (10) and (11) and $W_{ei,meas}$ is calculated from stationary measurements as $W_{ei,meas} = W_c/(1-x_{egr})$. Stationary measurements are used as inputs to the model during the tuning. The result of the tuning is shown in Fig. 2 that shows that the cylinder mass flow model has small absolute relative errors with a mean and a maximum absolute relative error of 0.9 % and 2.5 % respectively.

3.2 Exhaust manifold temperature

The exhaust manifold temperature model consists of a model for the cylinder out temperature and a model for the heat losses in the exhaust pipes.

Cylinder out temperature

The cylinder out temperature T_e is modeled in the same way as in Skogtjärn [17]. This approach is based upon ideal gas Seliger cycle (or limited pressure

cycle [11]) calculations that give the cylinder out temperature

$$T_e = \eta_{sc}\,\Pi_e^{1-1/\gamma_a}\,r_c^{1-\gamma_a}\,x_p^{1/\gamma_a-1}\left(q_{in}\left(\frac{1-x_{cv}}{c_{pa}}+\frac{x_{cv}}{c_{va}}\right)+T_1\,r_c^{\gamma_a-1}\right) \tag{16}$$

where η_{sc} is a compensation factor for non ideal cycles and x_{cv} the ratio of fuel consumed during constant volume combustion. The rest of the fuel $(1 - x_{cv})$ is used during constant pressure combustion. The model (16) also includes the following 6 components: the pressure quotient over the cylinder

$$\Pi_e = \frac{p_{em}}{p_{im}} \tag{17}$$

the pressure quotient between point 3 (after combustion) and point 2 (before combustion) in the Seliger cycle

$$x_p = \frac{p_3}{p_2} = 1 + \frac{q_{in}\,x_{cv}}{c_{va}\,T_1\,r_c^{\gamma_a-1}} \tag{18}$$

the specific energy contents of the charge

$$q_{in} = \frac{W_f\,q_{HV}}{W_{ei}+W_f}\,(1-x_r) \tag{19}$$

the temperature at inlet valve closing after intake stroke and mixing

$$T_1 = x_r\,T_e + (1-x_r)\,T_{im} \tag{20}$$

the residual gas fraction

$$x_r = \frac{\Pi_e^{1/\gamma_a}\,x_p^{-1/\gamma_a}}{r_c\,x_v} \tag{21}$$

and the volume quotient between point 3 (after combustion) and point 2 (before combustion) in the Seliger cycle

$$x_v = \frac{v_3}{v_2} = 1 + \frac{q_{in}\,(1-x_{cv})}{c_{pa}\left(\frac{q_{in}\,x_{cv}}{c_{va}}+T_1\,r_c^{\gamma_a-1}\right)} \tag{22}$$

Solution to the cylinder out temperature

Since the equations above are non-linear and depend on each other, the cylinder out temperature is calculated numerically using a fixed point iteration which starts with the initial values $x_{r,0}$ and $T_{1,0}$. Then the following equations are

applied in each iteration k

$$
\begin{aligned}
q_{in,k+1} &= \frac{W_f\, q_{HV}}{W_{ei} + W_f}\,(1 - x_{r,k}) \\
x_{p,k+1} &= 1 + \frac{q_{in,k+1}\, x_{cv}}{c_{va}\, T_{1,k}\, r_c^{\gamma_a - 1}} \\
x_{v,k+1} &= 1 + \frac{q_{in,k+1}\,(1 - x_{cv})}{c_{pa}\left(\frac{q_{in,k+1}\, x_{cv}}{c_{va}} + T_{1,k}\, r_c^{\gamma_a - 1}\right)} \\
x_{r,k+1} &= \frac{\Pi_e^{1/\gamma_a}\, x_{p,k+1}^{-1/\gamma_a}}{r_c\, x_{v,k+1}} \\
T_{e,k+1} &= \eta_{sc}\, \Pi_e^{1-1/\gamma_a}\, r_c^{1-\gamma_a}\, x_{p,k+1}^{1/\gamma_a - 1}\left(q_{in,k+1}\left(\frac{1 - x_{cv}}{c_{pa}} + \frac{x_{cv}}{c_{va}}\right) + T_{1,k}\, r_c^{\gamma_a - 1}\right) \\
T_{1,k+1} &= x_{r,k+1}\, T_{e,k+1} + (1 - x_{r,k+1})\, T_{im}
\end{aligned}
\tag{23}
$$

In each sample during the simulation, the initial values $x_{r,0}$ and $T_{1,0}$ are set to the solutions of x_r and T_1 from the previous sample.

Heat losses in the exhaust pipes

The cylinder out temperature model above does not describe the exhaust manifold temperature completely due to heat losses. This is illustrated in Fig. 3(a) which shows a comparison between measured and modeled exhaust manifold temperature and in this figure it is assumed that the exhaust manifold temperature is equal to the cylinder out temperature, i.e. $T_{em} = T_e$. The relative error between model and measurement seems to increase from a negative error to a positive error for increasing mass flow W_{eo} out from the cylinder. This is due to that the exhaust manifold temperature is measured in the exhaust manifold and that there are heat losses to the surroundings in the exhaust pipes between the cylinder and the exhaust manifold. Therefore the nest step is to include a sub-model for these heat losses.

This temperature drop is modeled in the same way as Model 1, presented in Eriksson [6], where the temperature drop is described as a function of mass flow out from the cylinder

$$
T_{em} = T_{amb} + (T_e - T_{amb})\, e^{-\frac{h_{tot}\,\pi\, d_{pipe}\, l_{pipe}\, n_{pipe}}{W_{eo}\, c_{pe}}} \tag{24}
$$

where T_{amb} is the ambient temperature, h_{tot} the total heat transfer coefficient, d_{pipe} the pipe diameter, l_{pipe} the pipe length and n_{pipe} the number of pipes. Using this model, the mean and maximum absolute relative error is reduced, see Fig. 3(b).

Approximating the solution to the cylinder out temperature

As explained above, the cylinder out temperature is calculated numerically using the fixed point iteration (23). A simulation of the complete engine model during the European Transient Cycle in Fig. 4 shows that it is sufficient to use one iteration in this iterative process. This is shown by comparing the solution from

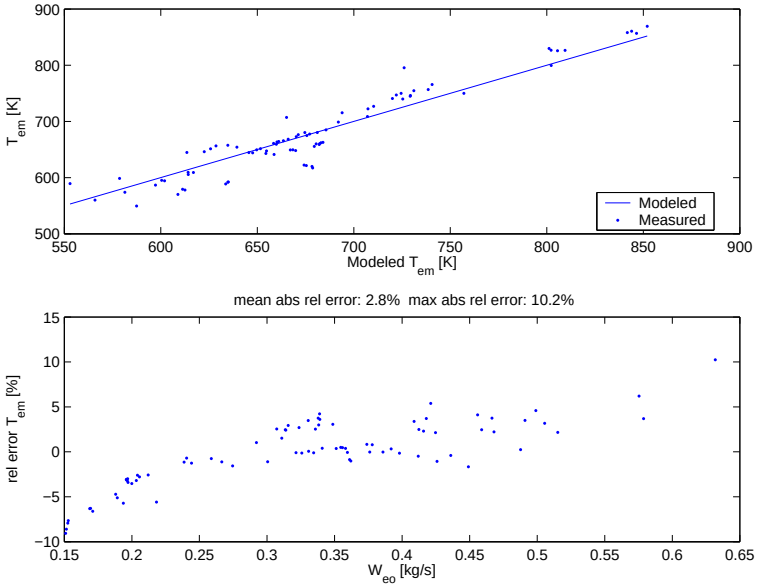

(a) Without a model for heat losses in the exhaust pipes, i.e. $T_{em} = T_e$.

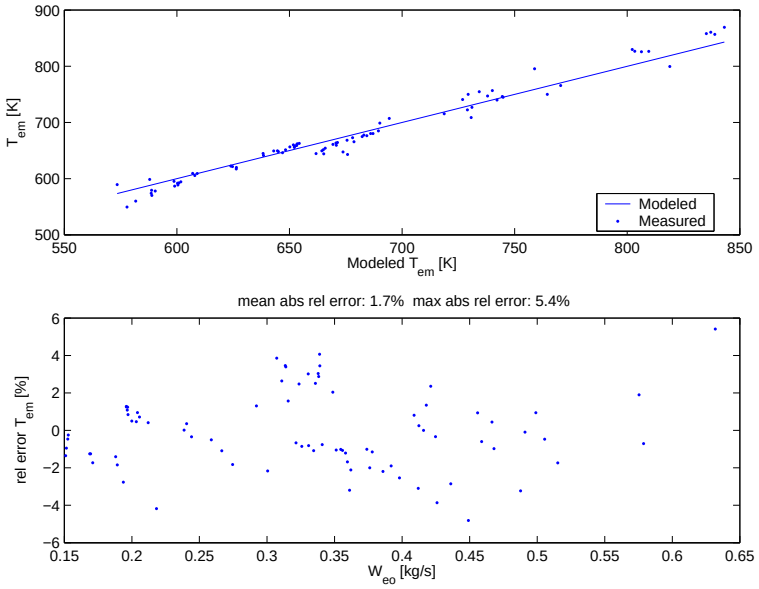

(b) With model (24) for heat losses in the exhaust pipes.

Figure 3: Modeled and measured exhaust manifold temperature T_{em} and relative errors for modeled T_{em} at steady state.

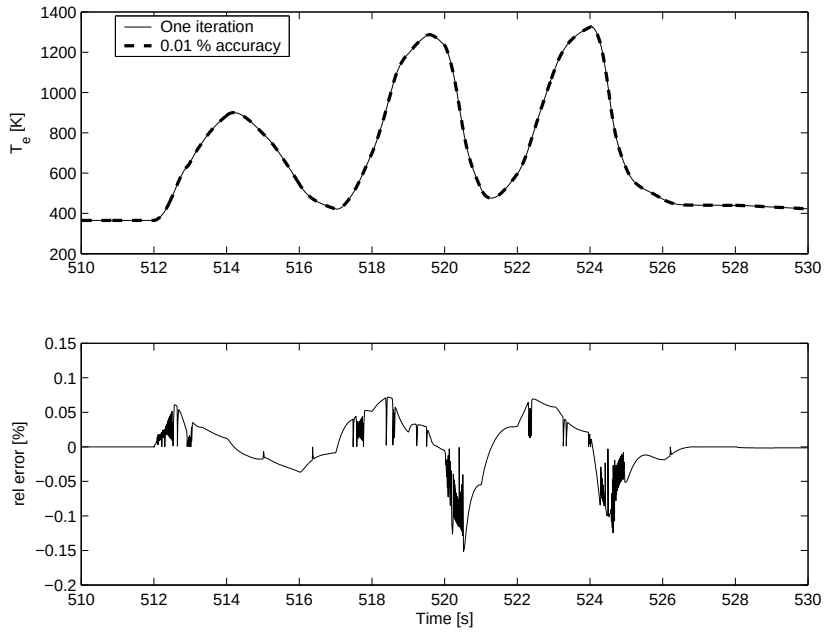

Figure 4: The cylinder out temperature T_e is calculated by simulating the total engine model during the complete European Transient Cycle. This figure shows the part of the European Transient Cycle that consists of the maximum relative error. **Top:** The fixed point iteration (23) is used in two ways: by using one iteration and to get 0.01 % accuracy. **Bottom:** Relative errors between the solutions from one iteration and 0.01 % accuracy.

one iteration with one that has sufficiently many iterations to give a solution with 0.01 % accuracy. The maximum absolute relative error of the solution from one iteration (compared to the solution with 0.01 % accuracy) is 0.15 %. This error is small because the fixed point iteration (23) has initial values that are close to the solution. Consequently, when using this method in simulation it is sufficient to use one iteration in this model since the mean absolute relative error of the exhaust manifold temperature model (compared to the measurements in Fig. 3(b)) is 1.7 %.

Tuning parameters

- η_{sc}: compensation factor for non ideal cycles
- x_{cv}: the ratio of fuel consumed during constant volume combustion
- h_{tot}: the total heat transfer coefficient

Tuning method

The tuning parameters η_{sc}, x_{cv}, and h_{tot} are determined by solving a non-linear least-squares problem that minimizes $(T_{em} - T_{em,meas})^2$ with η_{sc}, x_{cv}, and h_{tot} as the optimization variables. The variable T_{em} is the model in (23)

and (24) with stationary measurements as inputs to the model, and $T_{em,meas}$ is a stationary measurement. The result of the tuning is shown in Fig. 3(b) which shows that the model describes the exhaust manifold temperature well, with a mean and a maximum absolute relative error of 1.7 % and 5.4 % respectively.

3.3 Engine torque

The torque produced by the engine M_e is modeled using three different engine components; the gross indicated torque M_{ig}, the pumping torque M_p, and the friction torque M_{fric} [11].

$$M_e = M_{ig} - M_p - M_{fric} \tag{25}$$

The pumping torque is modeled using the intake and exhaust manifold pressures.

$$M_p = \frac{V_d}{4\,\pi}\left(p_{em} - p_{im}\right) \tag{26}$$

The gross indicated torque is coupled to the energy that comes from the fuel

$$M_{ig} = \frac{u_\delta\, 10^{-6}\, n_{cyl}\, q_{HV}\, \eta_{ig}}{4\,\pi} \tag{27}$$

Assuming that the engine is always running at optimal injection timing, the gross indicated efficiency η_{ig} is modeled as

$$\eta_{ig} = \eta_{igch}\left(1 - \frac{1}{r_c^{\gamma_{cyl}-1}}\right) \tag{28}$$

where the parameter η_{igch} is estimated from measurements, r_c is the compression ratio, and γ_{cyl} is the specific heat capacity ratio for the gas in the cylinder. The friction torque is assumed to be a quadratic polynomial in engine speed [11].

$$M_{fric} = \frac{V_d}{4\,\pi} 10^5 \left(c_{fric1}\, n_{eratio}^2 + c_{fric2}\, n_{eratio} + c_{fric3}\right) \tag{29}$$

where

$$n_{eratio} = \frac{n_e}{1000} \tag{30}$$

Tuning parameters

- η_{igch}: combustion chamber efficiency
- c_{fric1}, c_{fric2}, c_{fric3}: coefficients in the polynomial function for the friction torque

Tuning method

The tuning parameters η_{igch}, c_{fric1}, c_{fric2}, and c_{fric3} are determined by solving a linear least-squares problem that minimizes $(M_e + M_p - M_{e,meas} - M_{p,meas})^2$ with the tuning parameters as the optimization variables. The model of $M_e + M_p$ is obtained by solving (25) for $M_e + M_p$ and $M_{e,meas} + M_{p,meas}$ is calculated from stationary measurements as $M_{e,meas} + M_{p,meas} = M_e + V_d(p_{em} - p_{im})/(4\pi)$. Stationary measurements are used as inputs to the model. The result of the tuning is shown in Fig. 5 which shows that the engine torque model has small absolute relative errors with a mean and a maximum absolute relative error of 1.9 % and 7.1 % respectively.

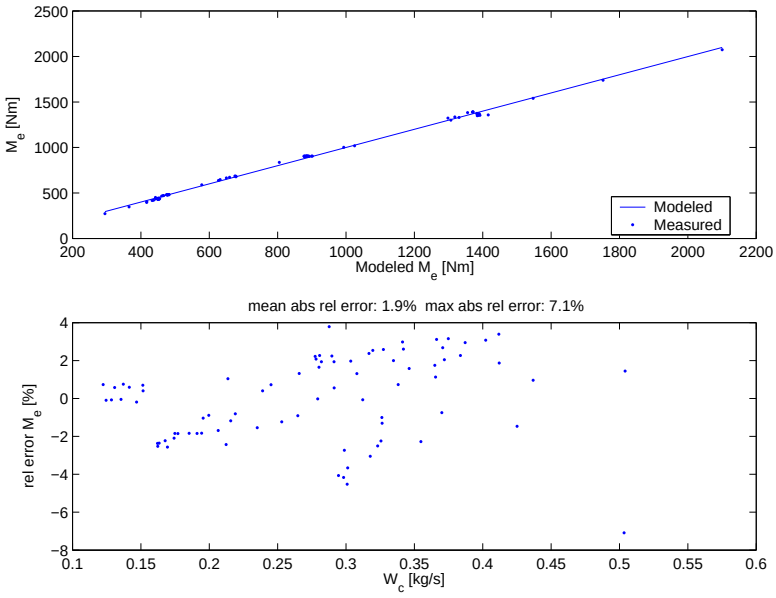

Figure 5: Comparison of measurements and model for the engine torque M_e at steady state. **Top:** Modeled and measured engine torque M_e. **Bottom:** Relative errors for modeled M_e.

4 EGR-valve

The EGR-valve model consists of sub-models for the EGR-valve mass flow and the EGR-valve actuator.

4.1 EGR-valve mass flow

The mass flow through the EGR-valve is modeled as a simplification of a compressible flow restriction with variable area [11] and with the assumption that there is no reverse flow when $p_{em} < p_{im}$. The motive for this assumption is to construct a simple model. The model can be extended with reverse flow, but this increases the complexity of the model since a reverse flow model requires mixing of different temperatures and oxygen fractions in the exhaust manifold and a change of the temperature and the gas constant in the EGR mass flow model. However, p_{em} is larger than p_{im} in normal operating points, consequently the assumption above will not effect the model behavior in these operating points. Furthermore, reverse flow is not measured and can therefore not be validated.

The mass flow through the restriction is

$$W_{egr} = \frac{A_{egr}\, p_{em}\, \Psi_{egr}}{\sqrt{T_{em}\, R_e}} \tag{31}$$

where

$$\Psi_{egr} = \sqrt{\frac{2\,\gamma_e}{\gamma_e - 1}\left(\Pi_{egr}^{2/\gamma_e} - \Pi_{egr}^{1+1/\gamma_e}\right)} \tag{32}$$

Measurement data shows that (32) does not give a sufficiently accurate description of the EGR flow. Pressure pulsations in the exhaust manifold or the

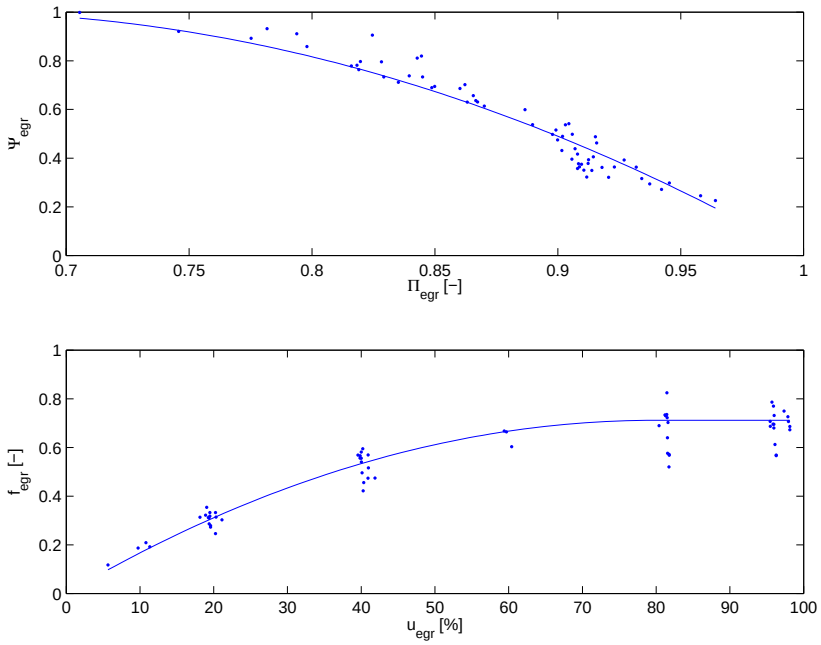

Figure 6: Comparison of calculated points from measurements and two sub-models for the EGR flow W_{egr} at steady state showing how different variables in the sub-models depend on each other. Note that this is not a validation of the sub-models since the calculated points for the sub-models depend on the model tuning. **Top:** The line shows Ψ_{egr} (33) as function of pressure quotient Π_{egr}. The data points are calculated by solving (31) for Ψ_{egr}. **Bottom:** The line shows the effective area ratio f_{egr} (37) as function of control signal u_{egr}. The data points are calculated by solving (31) for f_{egr}.

influence of the EGR-cooler could be two different explanations for this phenomenon. In order to maintain the density influence $(p_{em}/(\sqrt{T_{em}\, R_e}))$ in (31) and the simplicity in the model, the function Ψ_{egr} is instead modeled as a parabolic function (see Fig. 6 where Ψ_{egr} is plotted as function of Π_{egr}).

$$\Psi_{egr} = 1 - \left(\frac{1 - \Pi_{egr}}{1 - \Pi_{egropt}} - 1 \right)^2 \tag{33}$$

The pressure quotient Π_{egr} over the valve is limited when the flow is choked, i.e. when sonic conditions are reached in the throat, and when $1 < p_{im}/p_{em}$, i.e. no backflow can occur.

$$\Pi_{egr} = \begin{cases} \Pi_{egropt} & \text{if } \frac{p_{im}}{p_{em}} < \Pi_{egropt} \\ \frac{p_{im}}{p_{em}} & \text{if } \Pi_{egropt} \leq \frac{p_{im}}{p_{em}} \leq 1 \\ 1 & \text{if } 1 < \frac{p_{im}}{p_{em}} \end{cases} \tag{34}$$

For a compressible flow restriction, the standard model for Π_{egropt} is

$$\Pi_{egropt} = \left(\frac{2}{\gamma_e + 1} \right)^{\frac{\gamma_e}{\gamma_e - 1}} \tag{35}$$

but the accuracy of the EGR flow model is improved by replacing the physical value of Π_{egropt} in (35) with a tuning parameter [2].

The effective area

$$A_{egr} = A_{egrmax}\, f_{egr}(\tilde{u}_{egr}) \tag{36}$$

is modeled as a polynomial function of the EGR valve position $\tilde{u}_{egr}$ (see Fig. 6 where f_{egr} is plotted as function of u_{egr})

$$f_{egr}(\tilde{u}_{egr}) = \begin{cases} c_{egr1}\,\tilde{u}_{egr}^2 + c_{egr2}\,\tilde{u}_{egr} + c_{egr3} & \text{if } \tilde{u}_{egr} \leq -\frac{c_{egr2}}{2\,c_{egr1}} \\ c_{egr3} - \frac{c_{egr2}^2}{4\,c_{egr1}} & \text{if } \tilde{u}_{egr} > -\frac{c_{egr2}}{2\,c_{egr1}} \end{cases} \tag{37}$$

where $\tilde{u}_{egr}$ describes the EGR actuator dynamics, see Sec. 4.2. The EGR-valve is open when $\tilde{u}_{egr} = 100\%$ and closed when $\tilde{u}_{egr} = 0\%$.

Tuning parameters

- Π_{egropt}: optimal value of Π_{egr} for maximum value of the function Ψ_{egr} in (33)
- c_{egr1}, c_{egr2}, c_{egr3}: coefficients in the polynomial function for the effective area

Tuning method

The tuning parameters above are determined by solving a separable non-linear least-squares problem, see Björk [3] for details about the solution method. The non-linear part of this problem minimizes $(W_{egr} - W_{egr,meas})^2$ with Π_{egropt} as the optimization variable. In each iteration in the non-linear least-squares solver, the values for c_{egr1}, c_{egr2}, and c_{egr3} are set to be the solution of a linear least-squares problem that minimizes $(W_{egr} - W_{egr,meas})^2$ for the current value of Π_{egropt}. The variable W_{egr} is described by the model (31) and $W_{egr,meas}$ is calculated from measurements as $W_{egr,meas} = W_c\, x_{egr}/(1 - x_{egr})$. Stationary measurements are used as inputs to the model. The result of the tuning is shown in Fig. 7 which shows that the absolute relative errors are larger than 15 % in some points. However, the model describes the EGR mass flow well in the other points, and the mean and maximum absolute relative error are equal to 6.1 % and 22.2 % respectively.

4.2 EGR-valve actuator

The EGR-valve actuator dynamics is modeled as a second order system with an overshoot and a time delay, see Fig. 8. This model consist of a subtraction between two first order systems with different gains and time constants according to

$$\tilde{u}_{egr} = K_{egr}\,\tilde{u}_{egr1} - (K_{egr} - 1)\tilde{u}_{egr2} \tag{38}$$

$$\frac{d}{dt}\,\tilde{u}_{egr1} = \frac{1}{\tau_{egr1}}(u_{egr}(t - \tau_{degr}) - \tilde{u}_{egr1}) \tag{39}$$

$$\frac{d}{dt}\,\tilde{u}_{egr2} = \frac{1}{\tau_{egr2}}(u_{egr}(t - \tau_{degr}) - \tilde{u}_{egr2}) \tag{40}$$

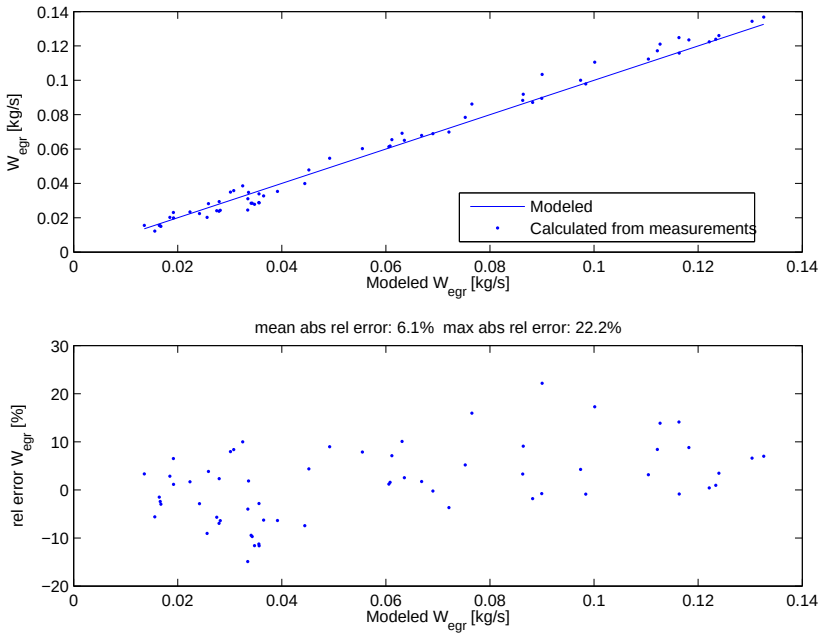

Figure 7: **Top:** Comparison between modeled EGR flow W_{egr} and calculated W_{egr} from measurements at steady state. **Bottom:** Relative errors for W_{egr} at steady state.

Tuning parameters

- τ_{egr1}, τ_{egr2}: time constants for the two different first order systems
- τ_{degr}: time delay
- K_{egr}: a parameter that affects the size of the overshoot

Tuning method

The tuning parameters above are determined by adjusting these parameters manually until simulations of the EGR-valve actuator model follow the dynamic responses in the dynamic data set J in Tab. 2. This data consist of 18 steps in EGR-valve position with a step size of 10% going from 0% up to 90% and then back again to 0% with a step size of 10%. The measurements also consist of 1 step with a step size of 30%, 1 step with a step size of 75%, 3 steps with a step size of 80%, and 1 step with a step size of 90%. These 24 steps are normalized and shifted in time in order to achieve the same starting point of the input step. These measurements are then compared with the unit step response for the linear system (38)-(40) in Fig. 8, which shows that the measurements have both large overshoots and no overshoots in some steps. However, the model describes the actuator well in average.

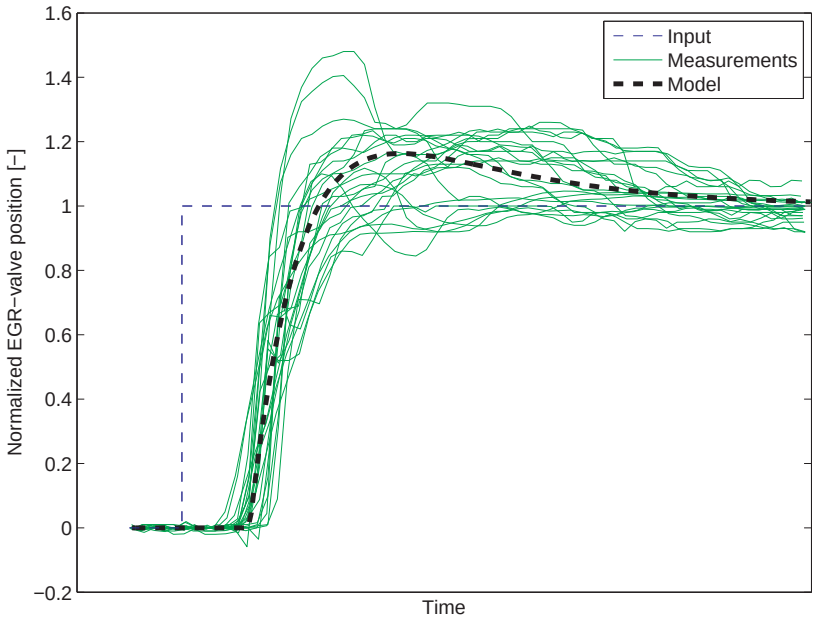

Figure 8: Comparison between EGR-actuator dynamic simulation and dynamic tuning data during steps in EGR-valve position.

5 Turbocharger

The turbocharger consists of a turbo inertia model, a turbine model, a VGT actuator model, and a compressor model.

5.1 Turbo inertia

For the turbo speed ω_t, Newton's second law gives

$$\frac{d}{dt}\omega_t = \frac{P_t\,\eta_m - P_c}{J_{tc}\,\omega_t} \tag{41}$$

where J_t is the inertia, P_t is the power delivered by the turbine, P_c is the power required to drive the compressor, and η_m is the mechanical efficiency in the turbocharger.

Tuning parameter

- J_t: turbo inertia

Tuning method

The tuning parameter J_t is determined by adjusting this parameter manually until simulations of the complete model follow the dynamic responses in the dynamic data set E in Tab. 2.

5.2 Turbine

The turbine model consists of sub-models for the total turbine efficiency and the turbine mass flow, which also includes the VGT actuator as a sub-model.

5.2.1 Turbine efficiency

One way to model the power P_t is to use the turbine efficiency η_t, which is defined as [11]

$$\eta_t = \frac{P_t}{P_{t,s}} = \frac{T_{em} - T_t}{T_{em}(1 - \Pi_t^{1-1/\gamma_e})} \tag{42}$$

where T_t is the temperature after the turbine, Π_t is the pressure ratio

$$\Pi_t = \frac{p_{amb}}{p_{em}} \tag{43}$$

and $P_{t,s}$ is the power from the isentropic process

$$P_{t,s} = W_t \, c_{pe} \, T_{em} \left(1 - \Pi_t^{1-1/\gamma_e}\right) \tag{44}$$

where W_t is the turbine mass flow.

In (42) it is assumed that there are no heat losses in the turbine, i.e. it is assumed that there are no temperature drops between the temperatures T_{em} and T_t that is due to heat losses. This assumption leads to errors in η_t if (42) is used to calculate η_t from measurements. One way to improve this model is to model these temperature drops, but it is difficult to tune these models since there exists no measurements of these temperature drops. Another way to improve the model, that is frequently used in the literature [7], is to use another efficiency that are approximatively equal to η_t. This approximation utilizes that

$$P_t \, \eta_m = P_c \tag{45}$$

at steady state according to (41). Consequently, $P_t \approx P_c$ at steady state. Using this approximation in (42), another efficiency η_{tm} is obtained

$$\eta_{tm} = \frac{P_c}{P_{t,s}} = \frac{W_c \, c_{pa}(T_c - T_{amb})}{W_t \, c_{pe} \, T_{em} \left(1 - \Pi_t^{1-1/\gamma_e}\right)} \tag{46}$$

where T_c is the temperature after the compressor and W_c is the compressor mass flow. The temperature T_{em} in (46) introduces less errors compared to the temperature difference $T_{em} - T_t$ in (42) due to that the absolute value of T_{em} is larger than the absolute value of $T_{em} - T_t$. Consequently, (46) introduces less errors compared to (42) since (46) does not consist of $T_{em} - T_t$. The temperatures T_c and T_{amb} are low and they introduce less errors compared to T_{em} and T_t since the heat losses in the compressor are comparatively small. Another advantage of using (46) is that the individual variables P_t and η_m in (41) do not have to be modeled. Instead, the product $P_t \, \eta_m$ is modeled using (45) and (46)

$$P_t \, \eta_m = \eta_{tm} \, P_{t,s} = \eta_{tm} \, W_t \, c_{pe} \, T_{em} \left(1 - \Pi_t^{1-1/\gamma_e}\right) \tag{47}$$

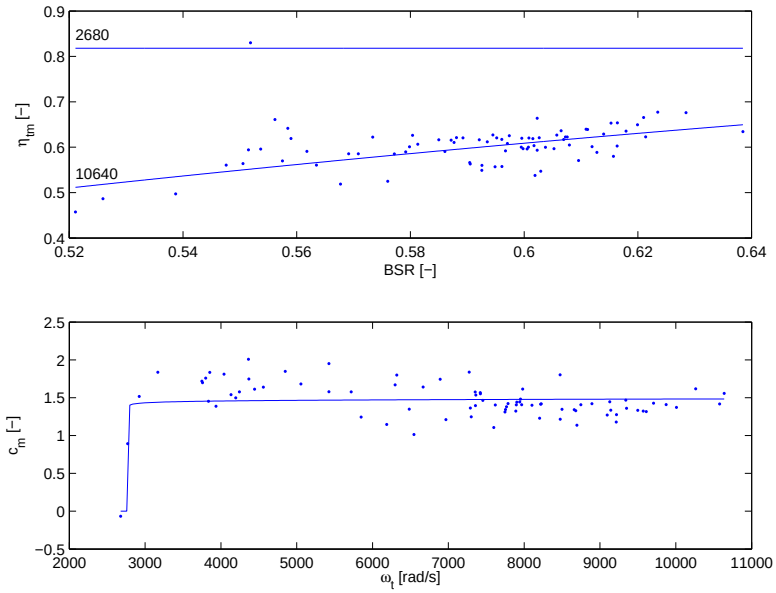

Figure 9: Comparison of calculated points from measurements and the model for the turbine efficiency η_{tm} at steady state. **Top:** The lines show η_{tm} (48) at two different turbo speeds as function of blade speed ratio BSR. The data points are calculated by using (46) and (49). **Bottom:** The line shows the parameter c_m (50) as function of turbo speed ω_t. The data points are calculated by solving (48) for c_m. Note that this plot is not a validation of c_m since the calculated points for c_m depend on the model tuning.

Measurements show that η_{tm} depends on the blade speed ratio (BSR) as a parabolic function [20], see Fig. 9 where η_{tm} is plotted as function of BSR.

$$\eta_{tm} = \eta_{tm,max} - c_m(BSR - BSR_{opt})^2 \tag{48}$$

The blade speed ratio is the quotient of the turbine blade tip speed and the speed which a gas reaches when expanded isentropically at the given pressure ratio Π_t

$$BSR = \frac{R_t\,\omega_t}{\sqrt{2\,c_{pe}\,T_{em}\left(1-\Pi_t^{1-1/\gamma_e}\right)}} \tag{49}$$

where R_t is the turbine blade radius. The parameter c_m in the parabolic function varies due to mechanical losses and c_m is therefore modeled as a function of the turbo speed

$$c_m = c_{m1}(\max(0, \omega_t - c_{m2}))^{c_{m3}} \tag{50}$$

see Fig. 9 where c_m is plotted as function of ω_t.

Tuning parameters

- $\eta_{tm,max}$: maximum turbine efficiency
- BSR_{opt}: optimum BSR value for maximum turbine efficiency

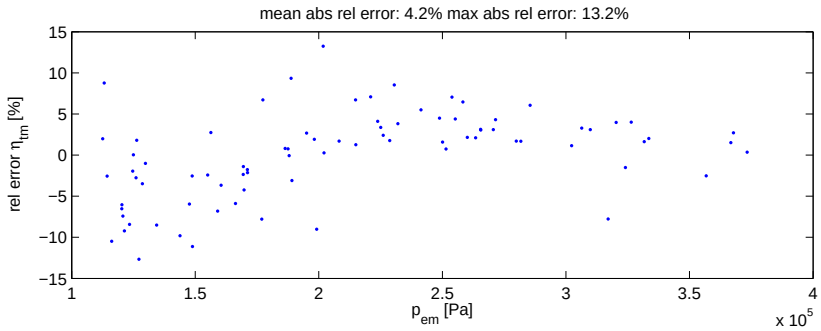

Figure 10: Relative errors for the total turbine efficiency η_{tm} as function of exhaust manifold pressure p_{em} at steady state.

- c_{m1}, c_{m2}, c_{m3}: parameters in the model for c_m

Tuning method

The tuning parameters above are determined by solving a separable non-linear least-squares problem, see Björk [3] for details about the solution method. The non-linear part of this problem minimizes $(\eta_{tm} - \eta_{tm,meas})^2$ with BSR_{opt}, c_{m2}, and c_{m3} as the optimization variables. In each iteration in the non-linear least-squares solver, the values for $\eta_{tm,max}$ and c_{m1} are set to be the solution of a linear least-squares problem that minimizes $(\eta_{tm} - \eta_{tm,meas})^2$ for the current values of BSR_{opt}, c_{m2}, and c_{m3}. The efficiency η_{tm} is described by the model (48) and $\eta_{tm,meas}$ is calculated from measurements using (46). Stationary measurements are used as inputs to the model. The result of the tuning is shown in Fig. 9 and 10 which show that the model describes the total turbine efficiency well with a mean and a maximum absolute relative error of 4.2 % and 13.2 % respectively.

5.2.2 Turbine mass flow

The turbine mass flow W_t is modeled using the corrected mass flow in order to consider density variations in the mass flow [11, 20]

$$\frac{W_t \sqrt{T_{em} R_e}}{p_{em}} = A_{vgtmax} f_{\Pi t}(\Pi_t) f_{vgt}(\tilde{u}_{vgt}) \tag{51}$$

where A_{vgtmax} is the maximum area in the turbine that the gas flows through. Measurements show that the corrected mass flow depends on the pressure ratio Π_t and the VGT actuator signal $\tilde{u}_{vgt}$. As the pressure ratio decreases, the corrected mass flow increases until the gas reaches the sonic condition and the flow is choked. This behavior can be described by a choking function

$$f_{\Pi t}(\Pi_t) = \sqrt{1 - \Pi_t^{K_t}} \tag{52}$$

which is not based on the physics of the turbine, but it gives good agreement with measurements using few parameters [8], see Fig. 11 where $f_{\Pi t}$ is plotted as function of Π_t.

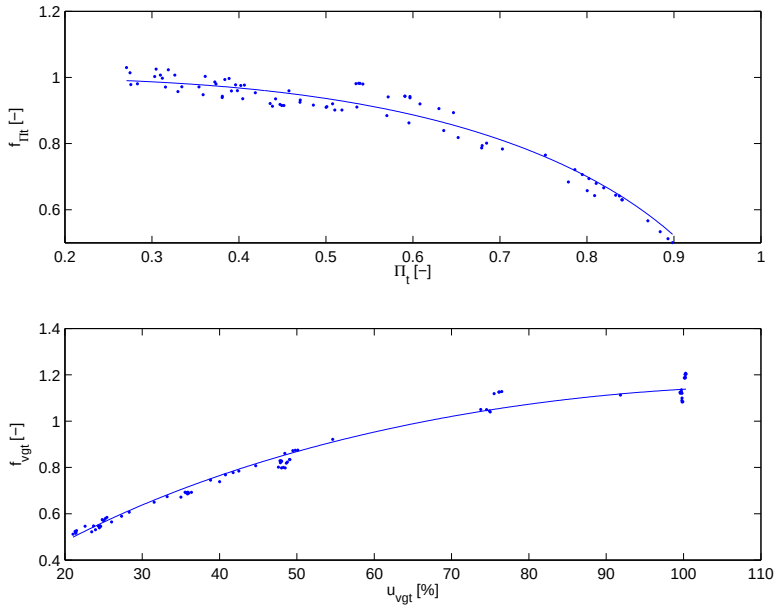

Figure 11: Comparison of calculated points from measurements and two sub-models for the turbine mass flow at steady state showing how different variables in the sub-models depend on each other. Note that this is not a validation of the sub-models since the calculated points for the sub-models depend on the model tuning. **Top:** The line shows the choking function $f_{\Pi t}$ (52) as function of the pressure ratio Π_t. The data points are calculated by solving (51) for $f_{\Pi t}$. **Bottom:** The line shows the effective area ratio function f_{vgt} (55) as function of the control signal u_{vgt}. The data points are calculated by solving (51) for f_{vgt}.

When the VGT control signal u_{vgt} increases, the effective area increases and hence also the flow increases. Due to the geometry in the turbine, the change in effective area is large when the VGT control signal is large. This behavior can be described by a part of an ellipse (see Fig. 11 where f_{vgt} is plotted as function of u_{vgt})

$$\left(\frac{f_{vgt}(\tilde{u}_{vgt}) - c_{f2}}{c_{f1}}\right)^2 + \left(\frac{\tilde{u}_{vgt} - c_{vgt2}}{c_{vgt1}}\right)^2 = 1 \tag{53}$$

where f_{vgt} is the effective area ratio function and $\tilde{u}_{vgt}$ describes the VGT actuator dynamics, see Sec. 5.2.3.

The value of τ_{vgt} has been provided by industry. The flow can now be modeled by solving (51) for W_t giving

$$W_t = \frac{A_{vgtmax}\, p_{em}\, f_{\Pi t}(\Pi_t)\, f_{vgt}(\tilde{u}_{vgt})}{\sqrt{T_{em}\, R_e}} \tag{54}$$

and solving (53) for f_{vgt} giving

$$f_{vgt}(\tilde{u}_{vgt}) = c_{f2} + c_{f1}\sqrt{\max(0, 1 - \left(\frac{\tilde{u}_{vgt} - c_{vgt2}}{c_{vgt1}}\right)^2)} \tag{55}$$

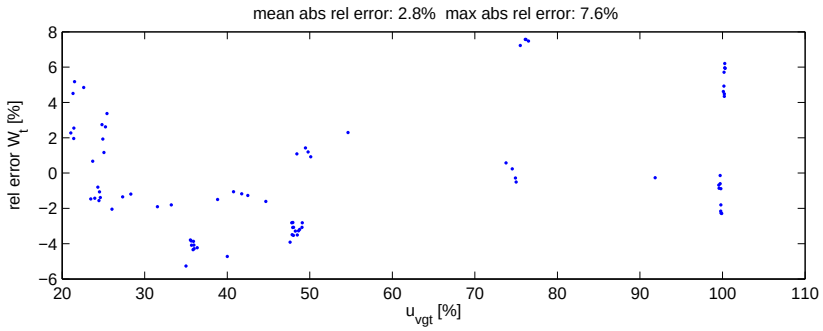

Figure 12: Relative errors for turbine flow W_t as function of control signal u_{vgt} at steady state.

Tuning parameters

- K_t: exponent in the choking function for the turbine flow
- c_{f1}, c_{f2}, c_{vgt1}, c_{vgt2}: parameters in the ellipse for the effective area ratio function

Tuning method

The tuning parameters above are determined by solving a non-linear least-squares problem that minimizes $(W_t - W_{t,meas})^2$ with the tuning parameters as the optimization variables. The flow W_t is described by the model (54), (55), and (52), and $W_{t,meas}$ is calculated from measurements as $W_{t,meas} = W_c + W_f$, where W_f is calculated using (12). Stationary measurements are used as inputs to the model. The result of the tuning is shown in Fig. 12 which shows small absolute relative errors with a mean and a maximum absolute relative error of 2.8 % and 7.6 % respectively.

5.2.3 VGT actuator

The VGT actuator dynamics is modeled as a first order system with a time delay according to

$$\frac{d}{dt}\,\tilde{u}_{vgt} = \frac{1}{\tau_{vgt}}(u_{vgt}(t - \tau_{dvgt}) - \tilde{u}_{vgt}) \tag{56}$$

Tuning parameters

- τ_{vgt}: time constant
- τ_{dvgt}: time delay

Tuning method

The tuning parameters above are determined by adjusting these parameters manually until simulations of the VGT actuator model follow the dynamic responses in the dynamic data set J in Tab. 2. This data consist of 18 steps in

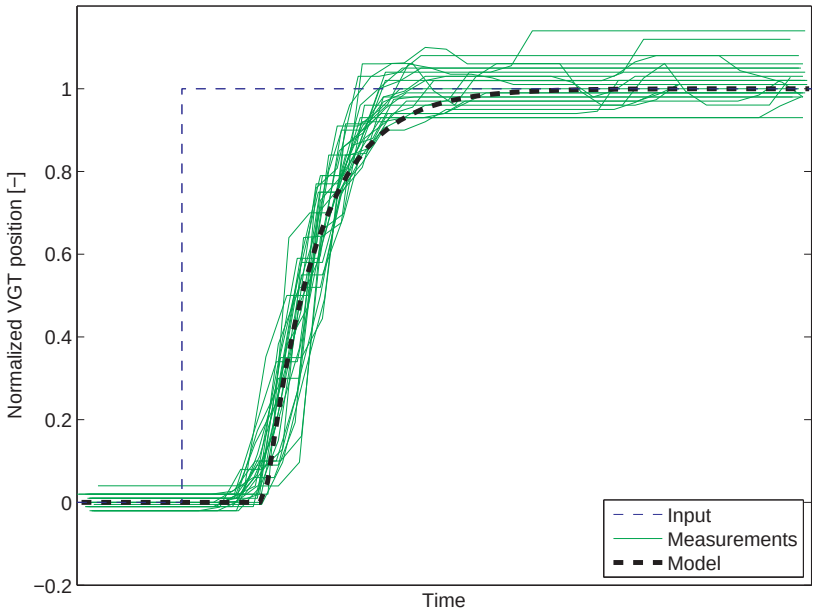

Figure 13: Comparison between VGT-actuator dynamic simulation and dynamic tuning data during steps in VGT position.

VGT position with a step size of 10% going from 100% down to 10% and then back again to 100% with a step size of 10%. The measurements also consist of 5 steps with a step size of 5% and 1 step with a step size of 20%. These 24 steps are then normalized and shifted in time in order to achieve the same starting point of the input step. These measurements are then compared with the unit step response for the linear system (56) in Fig. 13 which shows that the model describes the actuator well.

5.3 Compressor

The compressor model consists of sub-models for the compressor efficiency and the compressor mass flow.

5.3.1 Compressor efficiency

The compressor power P_c is modeled using the compressor efficiency η_c, which is defined as [11]

$$\eta_c = \frac{P_{c,s}}{P_c} = \frac{T_{amb}\left(\Pi_c^{1-1/\gamma_a} - 1\right)}{T_c - T_{amb}} \tag{57}$$

where T_c is the temperature after the compressor, Π_c is the pressure ratio

$$\Pi_c = \frac{p_{im}}{p_{amb}} \tag{58}$$

and $P_{c,s}$ is the power from the isentropic process

$$P_{c,s} = W_c\, c_{pa}\, T_{amb}\left(\Pi_c^{1-1/\gamma_a} - 1\right) \tag{59}$$

where W_c is the compressor mass flow. The power P_c is modeled by solving (57) for P_c and using (59)

$$P_c = \frac{P_{c,s}}{\eta_c} = \frac{W_c\, c_{pa}\, T_{amb}}{\eta_c} \left(\Pi_c^{1-1/\gamma_a} - 1 \right) \tag{60}$$

The efficiency is modeled using ellipses similar to Guzzella and Amstutz [9], but with a non-linear transformation on the axis for the pressure ratio similar to Andersson [2]. The inputs to the efficiency model are Π_c and W_c (see Fig. 18). The flow W_c is not scaled by the inlet temperature and the inlet pressure, in the current implementation, since these two variables are constant. However, this model can easily be extended with corrected mass flow in order to consider variations in the environmental conditions.

The ellipses can be described as

$$\eta_c = \eta_{cmax} - \chi^T\, Q_c\, \chi \tag{61}$$

χ is a vector which contains the inputs

$$\chi = \begin{bmatrix} W_c - W_{copt} \\ \pi_c - \pi_{copt} \end{bmatrix} \tag{62}$$

where the non-linear transformation for Π_c is

$$\pi_c = (\Pi_c - 1)^{c_\pi} \tag{63}$$

and the symmetric and positive definite matrix Q_c consists of three parameters

$$Q_c = \begin{bmatrix} a_1 & a_3 \\ a_3 & a_2 \end{bmatrix} \tag{64}$$

Tuning model parameters

- η_{cmax}: maximum compressor efficiency
- W_{copt} and π_{copt}: optimum values of W_c and π_c for maximum compressor efficiency
- c_π: exponent in the scale function, (63)
- a_1, a_2 and a_3: parameters in the matrix Q_c

Tuning method

The tuning parameters above are determined by solving a separable non-linear least-squares problem, see Björk [3] for details about the solution method. The non-linear part of this problem minimizes $(\eta_c - \eta_{c,meas})^2$ with W_{copt}, π_{copt}, and c_π as the optimization variables. In each iteration in the non-linear least-squares solver, the values for η_{cmax}, a_1, a_2 and a_3 are set to be the solution of a linear least-squares problem that minimizes $(\eta_c - \eta_{c,meas})^2$ for the current values of W_{copt}, π_{copt}, and c_π. The efficiency η_c is described by the model (61) to (64) and $\eta_{c,meas}$ is calculated from measurements using (57). Stationary measurements are used as inputs to the model. This method does not guarantee that the

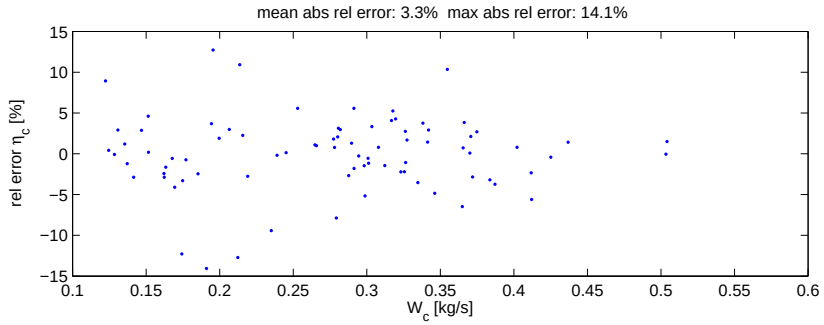

Figure 14: Relative errors for η_c as function of W_c at steady state.

matrix Q_c becomes positive definite, therefore it is important to check that Q_c is positive definite after the tuning. For the stationary tuning data in Sec. 1.4.1 Q_c is positive definite. The result of the tuning is shown in Fig. 14 which shows small absolute relative errors with a mean and a maximum absolute relative error of 3.3 % and 14.1 % respectively.

5.3.2 Compressor mass flow

The mass flow W_c through the compressor is modeled using two dimensionless variables. The first variable is the energy transfer coefficient [5]

$$\Psi_c = \frac{2\, c_{pa}\, T_{amb} \left(\Pi_c^{1-1/\gamma_a} - 1 \right)}{R_c^2\, \omega_t^2} \tag{65}$$

which is the quotient of the isentropic kinetic energy of the gas at the given pressure ratio Π_c and the kinetic energy of the compressor blade tip where R_c is compressor blade radius. The second variable is the volumetric flow coefficient [5]

$$\Phi_c = \frac{W_c/\rho_{amb}}{\pi\, R_c^3\, \omega_t} = \frac{R_a\, T_{amb}}{p_{amb}\, \pi\, R_c^3\, \omega_t} W_c \tag{66}$$

which is the quotient of volume flow rate of air into the compressor and the rate at which volume is displaced by the compressor blade where ρ_{amb} is the density of the ambient air. The relation between Ψ_c and Φ_c can be described by a part of an ellipse [2, 7], see Fig. 15 where Φ_c is plotted as function of Ψ_c

$$c_{\Psi 1}(\omega_t) \left(\Psi_c - c_{\Psi 2} \right)^2 + c_{\Phi 1}(\omega_t) \left(\Phi_c - c_{\Phi 2} \right)^2 = 1 \tag{67}$$

where $c_{\Psi 1}$ and $c_{\Phi 1}$ varies with turbo speed ω_t and are modeled as polynomial functions.

$$c_{\Psi 1}(\omega_t) = c_{\omega \Psi 1}\, \omega_t^2 + c_{\omega \Psi 2}\, \omega_t + c_{\omega \Psi 3} \tag{68}$$

$$c_{\Phi 1}(\omega_t) = c_{\omega \Phi 1}\, \omega_t^2 + c_{\omega \Phi 2}\, \omega_t + c_{\omega \Phi 3} \tag{69}$$

In Fig. 16 the variables $c_{\Psi 1}$ and $c_{\Phi 1}$ are plotted as function of the turbo speed ω_t.

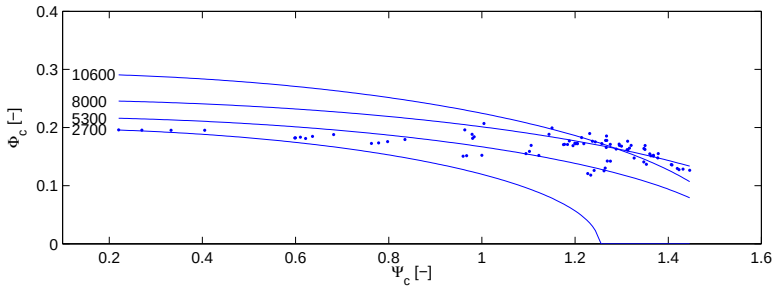

Figure 15: Comparison of calculated points from measurements and model for the compressor mass flow W_c at steady state. The lines show the volumetric flow coefficient Φ_c (70) at four different turbo speeds as function of energy transfer coefficient Ψ_c. The data points are calculated using (65) and (66).

The mass flow is modeled by solving (67) for Φ_c and solving (66) for W_c.

$$\Phi_c = \sqrt{\max\left(0, \frac{1 - c_{\Psi 1}\left(\Psi_c - c_{\Psi 2}\right)^2}{c_{\Phi 1}}\right)} + c_{\Phi 2} \tag{70}$$

$$W_c = \frac{p_{amb}\,\pi\,R_c^3\,\omega_t}{R_a\,T_{amb}}\Phi_c \tag{71}$$

Tuning model parameters

- $c_{\Psi 2}$, $c_{\Phi 2}$: parameters in the ellipse model for the compressor mass flow
- $c_{\omega\Psi 1}$, $c_{\omega\Psi 2}$, $c_{\omega\Psi 3}$: coefficients in the polynomial function (68)
- $c_{\omega\Phi 1}$, $c_{\omega\Phi 2}$, $c_{\omega\Phi 3}$: coefficients in the polynomial function (69)

Tuning method

The tuning parameters above are determined by solving a separable non-linear least-squares problem, see Björk [3] for details about the solution method. The non-linear part of this problem minimizes

$$\left(c_{\Psi 1}(\omega_t)\left(\Psi_c - c_{\Psi 2}\right)^2 + c_{\Phi 1}(\omega_t)\left(\Phi_c - c_{\Phi 2}\right)^2 - 1\right)^2$$

with $c_{\Psi 2}$ and $c_{\Phi 2}$ as the optimization variables. In each iteration in the non-linear least-squares solver, the values for $c_{\omega\Psi 1}$, $c_{\omega\Psi 2}$, $c_{\omega\Psi 3}$, $c_{\omega\Phi 1}$, $c_{\omega\Phi 2}$, and $c_{\omega\Phi 3}$ are set to be the solution of a linear least-squares problem that minimizes $\left(c_{\Psi 1}(\omega_t)\left(\Psi_c - c_{\Psi 2}\right)^2 + c_{\Phi 1}(\omega_t)\left(\Phi_c - c_{\Phi 2}\right)^2 - 1\right)^2$ for the current values of $c_{\Psi 2}$ and $c_{\Phi 2}$. Stationary measurements are used as inputs to the model. The result of the tuning is shown in Fig. 17 which shows that the model describes the compressor mass flow well with a mean and a maximum absolute relative error of 3.4 % and 13.7 % respectively.

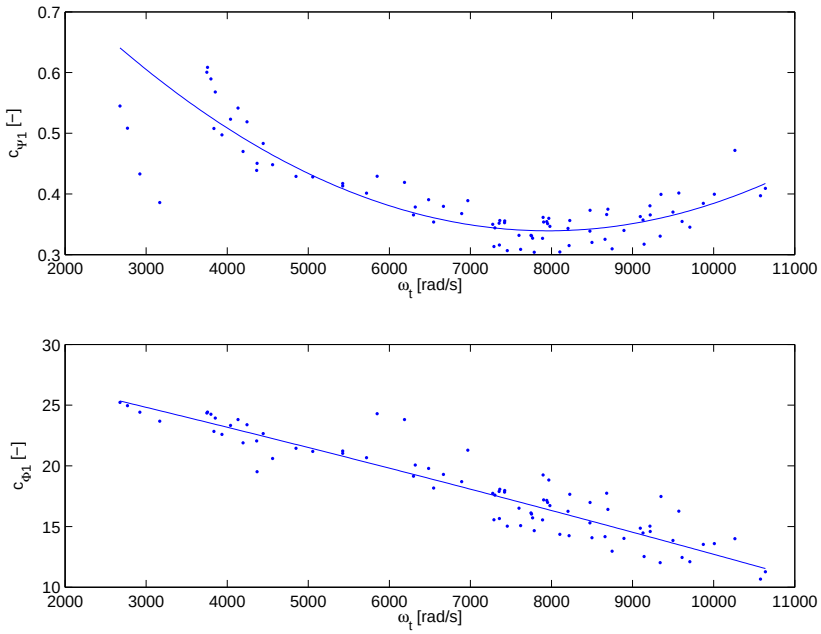

Figure 16: Comparison of calculated points from measurements and two sub-models for the compressor mass flow at steady state showing how different variables in the sub-models depend on each other. Note that this is not a validation of the sub-models since the calculated points for the sub-models depend on the model tuning. The lines show the sub-models $c_{\Psi 1}$ (68) and $c_{\Phi 1}$ (69) as function of turbo speed ω_t. The data points are calculated by solving (67) for $c_{\Psi 1}$ and $c_{\Phi 1}$.

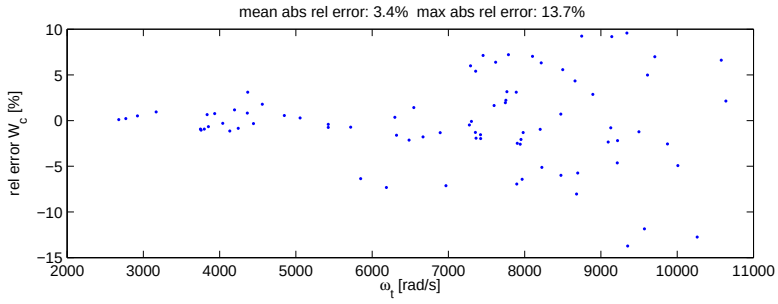

Figure 17: Relative errors for compressor flow W_c as function of turbocharger speed ω_t at steady state.

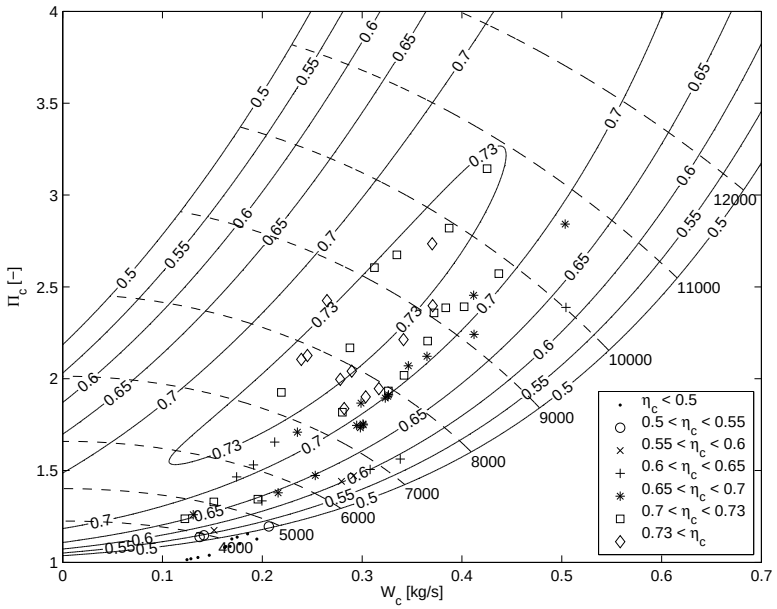

Figure 18: Compressor map with modeled efficiency lines (solid line), modeled turbo speed lines (dashed line with turbo speed in rad/s), and calculated efficiency from measurements using (57). The calculated points are divided into different groups. The turbo speed lines are described by the compressor flow model.

5.3.3 Compressor map

Compressor performance is usually presented in terms of a map with Π_c and W_c on the axes showing lines of constant efficiency and constant turbo speed. This is shown in Fig. 18 which has approximatively the same characteristics as Fig. 2.10 in Watson and Janota [20]. Consequently, the proposed model of the compressor efficiency (61) and the compressor flow (71) has the expected behavior.

6 Intercooler and EGR-cooler

To construct a simple model, that captures the important system properties, the intercooler and the EGR-cooler are assumed to be ideal, i.e. there is no pressure loss, no mass accumulation, and perfect efficiency, which give the following equations

$$\begin{aligned} p_{out} &= p_{in} \\ W_{out} &= W_{in} \\ T_{out} &= T_{cool} \end{aligned} \tag{72}$$

where T_{cool} is the cooling temperature. The model can be extended with non-ideal coolers, but these increase the complexity of the model since non-ideal

coolers require that there are states for the pressures both before and after the coolers.

7 Summary of assumptions and model equations

A summary of the model assumptions is given in Sec. 7.1 and the proposed model equations are given in Sec. 7.2 to 7.5.

7.1 Assumptions

To develop a simple model, that captures the dominating effects in the mass flows, the following assumptions were made:

1. The manifolds are modeled as standard isothermal models.
2. All gases are considered to be ideal and there are two sets of thermodynamic properties:
   (a) Air has the gas constant R_a and the specific heat capacity ratio γ_a.
   (b) Exhaust gas has the gas constant R_e and the specific heat capacity ratio γ_e.
3. The EGR gas in the intake manifold affects neither the gas constant nor the specific heat capacity in the intake manifold.
4. No heat transfer to or from the gas inside of the intake manifold.
5. No backflow can occur in the EGR-valve, compressor, turbine, or the cylinder.
6. The oxygen fuel ratio λ_O is always larger than one.
7. The intercooler and the EGR-cooler are ideal, i.e. the equations for the coolers are

$$\begin{aligned} p_{out} &= p_{in} \\ W_{out} &= W_{in} \\ T_{out} &= T_{cool} \end{aligned} \tag{73}$$

   where T_{cool} is the cooling temperature.

Note that assumptions 1 and 7 above lead to that the intake manifold temperature is constant.

7.2 Manifolds

$$\begin{aligned} \frac{d}{dt} p_{im} &= \frac{R_a T_{im}}{V_{im}} (W_c + W_{egr} - W_{ei}) \\ \frac{d}{dt} p_{em} &= \frac{R_e T_{em}}{V_{em}} (W_{eo} - W_t - W_{egr}) \end{aligned} \tag{74}$$

$$x_{egr} = \frac{W_{egr}}{W_c + W_{egr}} \tag{75}$$

$$\begin{aligned}\frac{d}{dt}X_{Oim} &= \frac{R_a\,T_{im}}{p_{im}\,V_{im}}\left(\left(X_{Oem}-X_{Oim}\right)W_{egr}+\left(X_{Oc}-X_{Oim}\right)W_c\right)\\ \frac{d}{dt}X_{Oem} &= \frac{R_e\,T_{em}}{p_{em}\,V_{em}}\left(X_{Oe}-X_{Oem}\right)W_{eo}\end{aligned} \tag{76}$$

7.3 Cylinder

7.3.1 Cylinder flow

$$W_{ei} = \frac{\eta_{vol}\,p_{im}\,n_e\,V_d}{120\,R_a\,T_{im}} \tag{77}$$

$$\eta_{vol} = c_{vol1}\sqrt{p_{im}} + c_{vol2}\sqrt{n_e} + c_{vol3} \tag{78}$$

$$W_f = \frac{10^{-6}}{120}\,u_\delta\,n_e\,n_{cyl} \tag{79}$$

$$W_{eo} = W_f + W_{ei} \tag{80}$$

$$\lambda_O = \frac{W_{ei}\,X_{Oim}}{W_f\,(O/F)_s} \tag{81}$$

$$X_{Oe} = \frac{W_{ei}\,X_{Oim} - W_f\,(O/F)_s}{W_{eo}} \tag{82}$$

7.3.2 Cylinder out temperature

$$\begin{aligned}q_{in,k+1} &= \frac{W_f\,q_{HV}}{W_{ei}+W_f}\left(1-x_{r,k}\right)\\ x_{p,k+1} &= 1+\frac{q_{in,k+1}\,x_{cv}}{c_{va}\,T_{1,k}\,r_c^{\gamma_a-1}}\\ x_{v,k+1} &= 1+\frac{q_{in,k+1}\left(1-x_{cv}\right)}{c_{pa}\left(\frac{q_{in,k+1}\,x_{cv}}{c_{va}}+T_{1,k}\,r_c^{\gamma_a-1}\right)}\\ x_{r,k+1} &= \frac{\Pi_e^{1/\gamma_a}\,x_{p,k+1}^{-1/\gamma_a}}{r_c\,x_{v,k+1}}\\ T_{e,k+1} &= \eta_{sc}\,\Pi_e^{1-1/\gamma_a}\,r_c^{1-\gamma_a}\,x_{p,k+1}^{1/\gamma_a-1}\left(q_{in,k+1}\left(\frac{1-x_{cv}}{c_{pa}}+\frac{x_{cv}}{c_{va}}\right)+T_{1,k}\,r_c^{\gamma_a-1}\right)\\ T_{1,k+1} &= x_{r,k+1}\,T_{e,k+1}+\left(1-x_{r,k+1}\right)T_{im}\end{aligned} \tag{83}$$

$$T_{em} = T_{amb} + \left(T_e - T_{amb}\right)e^{-\frac{h_{tot}\,\pi\,d_{pipe}\,l_{pipe}\,n_{pipe}}{W_{eo}\,c_{pe}}} \tag{84}$$

7.3.3 Cylinder torque

$$M_e = M_{ig} - M_p - M_{fric} \tag{85}$$

$$M_p = \frac{V_d}{4\,\pi}\left(p_{em}-p_{im}\right) \tag{86}$$

$$M_{ig} = \frac{u_\delta\,10^{-6}\,n_{cyl}\,q_{HV}\,\eta_{ig}}{4\,\pi} \tag{87}$$

$$\eta_{ig} = \eta_{igch}\left(1 - \frac{1}{r_c^{\gamma_{cyl}-1}}\right) \tag{88}$$

$$M_{fric} = \frac{V_d}{4\,\pi} 10^5 \ \left(c_{fric1}\, n_{eratio}^2 + c_{fric2}\, n_{eratio} + c_{fric3}\right) \tag{89}$$

$$n_{eratio} = \frac{n_e}{1000} \tag{90}$$

7.4 EGR-valve

$$W_{egr} = \frac{A_{egr}\, p_{em}\, \Psi_{egr}}{\sqrt{T_{em}\, R_e}} \tag{91}$$

$$\Psi_{egr} = 1 - \left(\frac{1 - \Pi_{egr}}{1 - \Pi_{egropt}} - 1\right)^2 \tag{92}$$

$$\Pi_{egr} = \begin{cases} \Pi_{egropt} & \text{if } \frac{p_{im}}{p_{em}} < \Pi_{egropt} \\ \frac{p_{im}}{p_{em}} & \text{if } \Pi_{egropt} \leq \frac{p_{im}}{p_{em}} \leq 1 \\ 1 & \text{if } 1 < \frac{p_{im}}{p_{em}} \end{cases} \tag{93}$$

$$A_{egr} = A_{egrmax}\, f_{egr}(\tilde{u}_{egr}) \tag{94}$$

$$f_{egr}(\tilde{u}_{egr}) = \begin{cases} c_{egr1}\, \tilde{u}_{egr}^2 + c_{egr2}\, \tilde{u}_{egr} + c_{egr3} & \text{if } \tilde{u}_{egr} \leq -\frac{c_{egr2}}{2\, c_{egr1}} \\ c_{egr3} - \frac{c_{egr2}^2}{4\, c_{egr1}} & \text{if } \tilde{u}_{egr} > -\frac{c_{egr2}}{2\, c_{egr1}} \end{cases} \tag{95}$$

$$\tilde{u}_{egr} = K_{egr}\, \tilde{u}_{egr1} - (K_{egr} - 1)\tilde{u}_{egr2} \tag{96}$$

$$\frac{d}{dt}\, \tilde{u}_{egr1} = \frac{1}{\tau_{egr1}}(u_{egr}(t - \tau_{degr}) - \tilde{u}_{egr1}) \tag{97}$$

$$\frac{d}{dt}\, \tilde{u}_{egr2} = \frac{1}{\tau_{egr2}}(u_{egr}(t - \tau_{degr}) - \tilde{u}_{egr2}) \tag{98}$$

7.5 Turbo

7.5.1 Turbo inertia

$$\frac{d}{dt}\omega_t = \frac{P_t\, \eta_m - P_c}{J_{tc}\, \omega_t} \tag{99}$$

7.5.2 Turbine efficiency

$$P_t\, \eta_m = \eta_{tm}\, W_t\, c_{pe}\, T_{em}\left(1 - \Pi_t^{1-1/\gamma_e}\right) \tag{100}$$

$$\Pi_t = \frac{p_{amb}}{p_{em}} \tag{101}$$

$$\eta_{tm} = \eta_{tm,max} - c_m(BSR - BSR_{opt})^2 \tag{102}$$

$$BSR = \frac{R_t\, \omega_t}{\sqrt{2\, c_{pe}\, T_{em}\left(1 - \Pi_t^{1-1/\gamma_e}\right)}} \tag{103}$$

$$c_m = c_{m1}(\max(0, \omega_t - c_{m2}))^{c_{m3}} \tag{104}$$

7.5.3 Turbine mass flow

$$W_t = \frac{A_{vgtmax}\, p_{em}\, f_{\Pi t}(\Pi_t)\, f_{vgt}(\tilde{u}_{vgt})}{\sqrt{T_{em}\, R_e}} \tag{105}$$

$$f_{\Pi t}(\Pi_t) = \sqrt{1 - \Pi_t^{K_t}} \tag{106}$$

$$f_{vgt}(\tilde{u}_{vgt}) = c_{f2} + c_{f1}\sqrt{\max\left(0, 1 - \left(\frac{\tilde{u}_{vgt} - c_{vgt2}}{c_{vgt1}}\right)^2\right)} \tag{107}$$

$$\frac{d}{dt}\,\tilde{u}_{vgt} = \frac{1}{\tau_{vgt}}(u_{vgt}(t - \tau_{dvgt}) - \tilde{u}_{vgt}) \tag{108}$$

7.5.4 Compressor efficiency

$$P_c = \frac{W_c\, c_{pa}\, T_{amb}}{\eta_c}\left(\Pi_c^{1-1/\gamma_a} - 1\right) \tag{109}$$

$$\Pi_c = \frac{p_{im}}{p_{amb}} \tag{110}$$

$$\eta_c = \eta_{cmax} - \chi^T\, Q_c\, \chi \tag{111}$$

$$\chi = \begin{bmatrix} W_c - W_{copt} \\ \pi_c - \pi_{copt} \end{bmatrix} \tag{112}$$

$$\pi_c = (\Pi_c - 1)^{c_\pi} \tag{113}$$

$$Q_c = \begin{bmatrix} a_1 & a_3 \\ a_3 & a_2 \end{bmatrix} \tag{114}$$

7.5.5 Compressor mass flow

$$W_c = \frac{p_{amb}\, \pi\, R_c^3\, \omega_t}{R_a\, T_{amb}}\Phi_c \tag{115}$$

$$\Phi_c = \sqrt{\max\left(0, \frac{1 - c_{\Psi 1}\,(\Psi_c - c_{\Psi 2})^2}{c_{\Phi 1}}\right)} + c_{\Phi 2} \tag{116}$$

$$\Psi_c = \frac{2\, c_{pa}\, T_{amb}\left(\Pi_c^{1-1/\gamma_a} - 1\right)}{R_c^2\, \omega_t^2} \tag{117}$$

$$c_{\Psi 1} = c_{\omega\Psi 1}\, \omega_t^2 + c_{\omega\Psi 2}\, \omega_t + c_{\omega\Psi 3} \tag{118}$$

$$c_{\Phi 1} = c_{\omega\Phi 1}\, \omega_t^2 + c_{\omega\Phi 2}\, \omega_t + c_{\omega\Phi 3} \tag{119}$$

Table 4: The mean and maximum absolute relative errors between static models and the stationary tuning data for each subsystem in the diesel engine model, i.e. a summary of the mean and maximum absolute relative errors in Sec. 3 to 5.

Subsystem	Mean absolute relative error [%]	Maximum absolute relative error [%]
Cylinder mass flow	0.9	2.5
Exhaust gas temperature	1.7	5.4
Engine torque	1.9	7.1
EGR mass flow	6.1	22.2
Turbine efficiency	4.2	13.2
Turbine mass flow	2.8	7.6
Compressor efficiency	3.3	14.1
Compressor mass flow	3.4	13.7

8 Model tuning and validation

One step in the development of a model that describes the system dynamics and the nonlinear effects is the tuning and validation. In Sec. 8.1 a summary of the model tuning is given and in Sec. 8.2 a validation of the complete model is performed using dynamic data. In the validation, it is important to investigate if the model captures the essential dynamic behaviors and nonlinear effects. The data that is used in the tuning and validation are described in Sec. 1.4.

8.1 Summary of tuning

A summary of the tuning of static and dynamic models and its results are given in the following sections. In order to validate the engine torque model during dynamic responses, a time constant for the engine torque is modeled and tuned in Sec. 8.1.2.

8.1.1 Static models

As described in Sec. 1.5, parameters in static models are estimated automatically using least squares optimization and tuning data from stationary measurements. The tuning methods for each parameter and the tuning results are described in Sec. 3 to 5. The tuning results are summarized in Tab. 4 showing the absolute relative model errors between static sub-models and stationary tuning data. The mean absolute relative errors are 6.1 % or lower. The EGR mass flow model has the largest mean absolute relative error and the cylinder mass flow model has the smallest mean absolute relative error.

8.1.2 Dynamic models

As described in Sec. 1.5, parameters in dynamic models are estimated in two steps. Firstly, the actuator parameters are estimated using the method in Sec. 4.2 and 5.2.3. These sections also show the tuning results for the actuators. Secondly, the manifold volumes and the turbocharger inertia are estimated using the method in Sec. 2 and 5.1. The tuning result of the second step is shown

Table 5: The mean absolute relative errors between diesel engine model simulation and dynamic tuning or validation data that consist of steps in VGT-position, EGR-valve, and fuel injection. The data sets E and I are used for tuning of dynamic models, the data sets A-D and F-I are used for validation of essential system properties and time constants, and all the data sets are used for validation of static models.

	VGT-EGR steps								u_δ steps
Data set	A	B	C	D	E	F	G	H	I
Speed [rpm]	1200				1500	1900			1500
Load [%]	25	40	50	75	50	25	75	100	-
Number of steps	77	35	2	77	77	77	55	1	7
p_{im}	2.0	1.6	7.2	10.6	6.3	5.0	4.5	4.9	2.9
p_{em}	2.4	4.7	4.9	6.8	5.5	4.5	4.6	4.8	4.7
W_c	3.2	4.7	5.6	10.7	8.0	6.7	6.7	7.4	3.8
n_t	4.4	8.9	4.6	11.9	7.0	6.0	4.1	12.7	3.0
M_e	-	-	-	-	-	-	-	-	7.3

in Tab. 5 for the data set E that shows that the mean absolute relative errors are 8 % or lower.

A dynamometer is fitted to the engine via an axle-shaft in order to brake or supply torque to the engine. This dynamometer and axle-shaft lead to that the measured engine torque has a time constant that is not modeled due to that the torque will not be used as a feedback in the controller. However, in order to validate the engine torque model during dynamic responses, this dynamics is modeled in the validation as a first order system

$$\frac{d}{dt} M_{e,meas} = \frac{1}{\tau_{Me}} (M_e - M_{e,meas}) \tag{120}$$

where $M_{e,meas}$ is the measured torque and M_e is the output torque from the engine. The time constant τ_{Me} is tuned by adjusting it manually until simulations of the complete model follow the measured torque during steps in fuel injection at 1500 rpm, i.e. the data set I in Tab. 5 which gives a mean absolute relative error of 7.3 % for the engine torque. The result of the tuning is shown in Fig. 19 showing that the model captures the dynamic in the engine torque.

8.2 Validation

Due to that the stationary measurements are few, both the static and the dynamic models are validated by simulating the total model and comparing it with the dynamic validation data sets A-I in Tab. 2. The result of this validation can be seen in Tab. 5 that shows that the mean absolute relative errors are 12.7 % or lower. Note that the engine torque is not measured during VGT and EGR steps. The relative errors are due to mostly steady state errors, but since the engine model will be used in a controller the steady state accuracy is less important since a controller will take care of steady state errors. However, in order to design a successful controller, it is important that the model captures the essential dynamic behaviors and nonlinear effects. Therefore, essential system properties and time constants are validated in the following section.

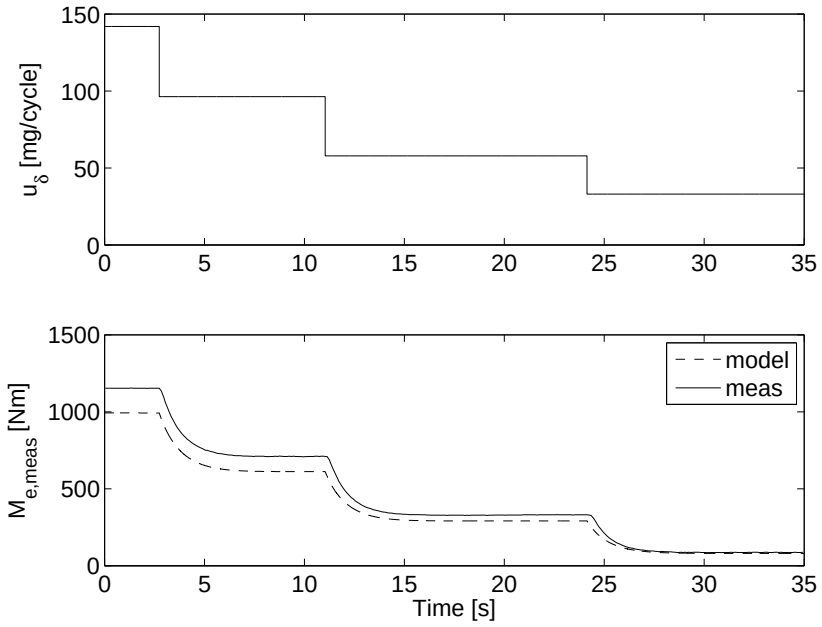

Figure 19: Comparison between diesel engine model simulation and dynamic tuning data during steps in fuel injection showing that the model captures the dynamic in $M_{e,meas}$. Data set I. Operating point: n_e=1500 rpm, u_{vgt}=26 %, and u_{egr}=19 %.

8.2.1 Validation of essential system properties and time constants

Kolmanovsky et al. [14] and Jung [13] show the essential system properties for the pressures and the flows in a diesel engine with VGT and EGR. Some of these properties are a non-minimum phase behavior in the intake manifold pressure and a non-minimum phase behavior, an overshoot, and a sign reversal in the compressor mass flow. These system properties and time constants are validated using the dynamic validation data sets A-D and F-I in Tab. 5. Three validations are performed in Fig. 20-22. Fig. 20 shows that the model captures the non-minimum phase behavior in the channel u_{egr} to p_{im}. Fig. 21 shows that the model captures the non-minimum phase behavior in the channel u_{vgt} to W_c. Fig. 22 shows that the model captures the overshoot in the channel u_{vgt} to W_c and a small non-minimum phase behavior in the channel u_{vgt} to n_t. Fig. 20 to 22 also show that the model captures the fast dynamics in the beginning of the responses and the slow dynamics in the end of the responses. Further, by comparing Fig. 21 and 22, it can be seen that the model captures the sign reversal in u_{vgt} to W_c. In Fig. 21 the DC-gain is negative and in Fig. 22 the DC-gain is positive.

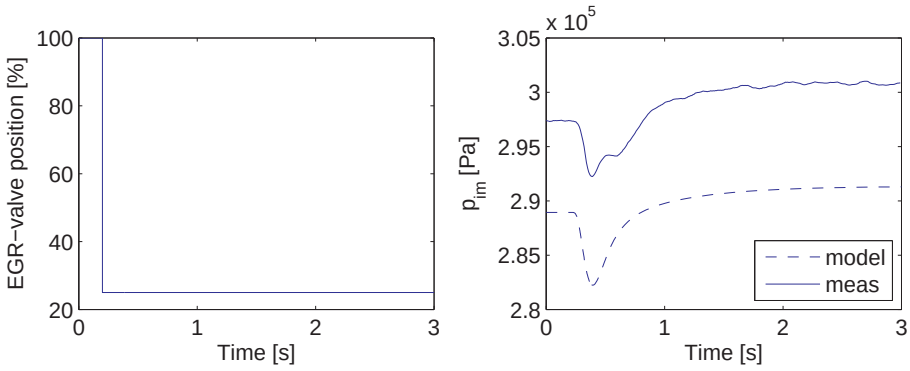

Figure 20: Comparison between diesel engine model simulation and dynamic validation data during a step in EGR-valve position showing that the model captures the non-minimum phase behavior in p_{im}. Data set H. Operating point: 100 % load, n_e=1900 rpm and u_{vgt}=60 %.

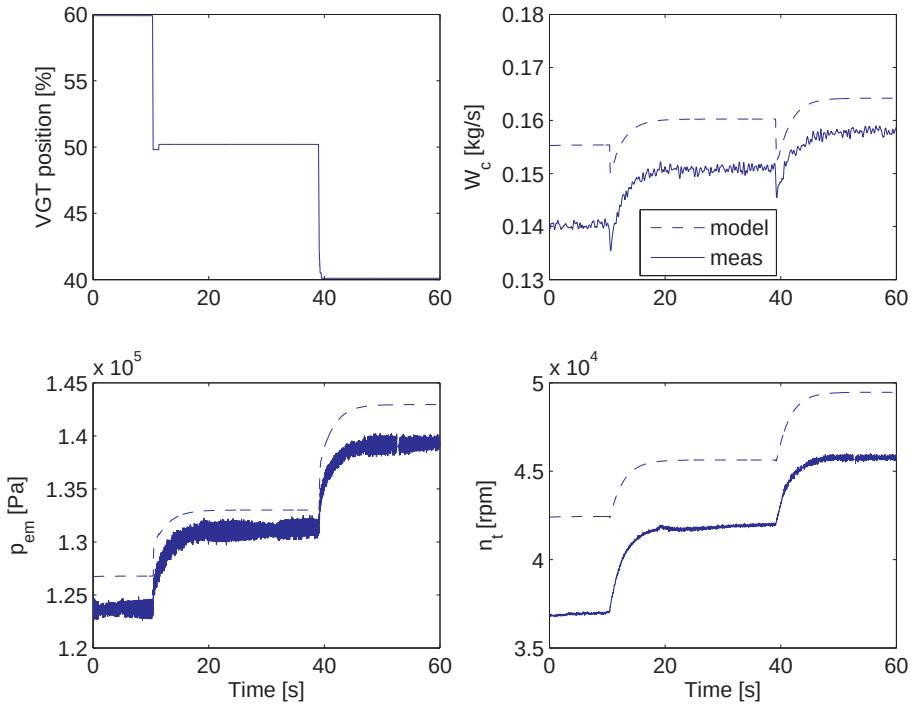

Figure 21: Comparison between diesel engine model simulation and dynamic validation data during steps in VGT position showing that the model captures the non-minimum phase behavior in W_c. Data set B. Operating point: 40 % load, n_e=1200 rpm and u_{egr}=100 %.

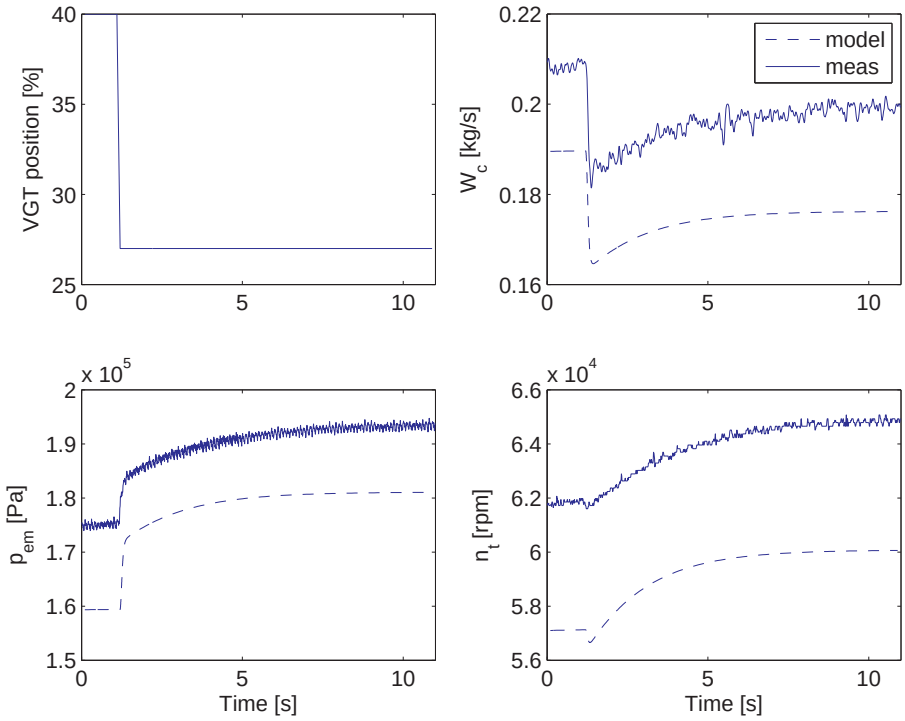

Figure 22: Comparison between diesel engine model simulation and dynamic validation data during a step in VGT position showing that the model captures the overshoot in W_c and a small non-minimum phase behavior in n_t. A comparison between Fig. 21 and 22 also shows that the model captures the sign reversal in W_c. Data set C. Operating point: 50 % load, n_e=1200 rpm and u_{egr}=100 %.

9 Model extensions

The proposed model in Sec. 2 to 8 is a small model with 8 states that describes the important dynamics and non-linear system properties according to Sec. 8. In the following sections the goal is to investigate if this model can be improved substantially with model extensions. In Sec. 9.1 the proposed model is extended with temperature states and in Sec. 9.2 the proposed model is extended with temperature states, a pressure drop over the intercooler, and an extra control volume.

9.1 Extensions: temperature states

To investigate if temperature states in the manifolds improve the model substantially, the 8:th order model in Sec. 2 to 6 is extended with two temperature states (T_{im} and T_{em}) which leads to a 10:th order model with the states

$$x = (p_{im} \quad p_{em} \quad T_{im} \quad T_{em} \quad X_{Oim} \quad X_{Oem} \quad \omega_t \quad \tilde{u}_{egr1} \quad \tilde{u}_{egr2} \quad \tilde{u}_{vgt})^T \tag{121}$$

9.1.1 Extended model equations

The intake and exhaust manifold models in Sec. 2 are extended with temperatures states T_{im} and T_{em} according to the adiabatic model [4, 10]

$$\begin{aligned}
&\frac{d}{dt} T_{im} = \frac{R_a T_{im}}{p_{im} V_{im} c_{va}} \cdot \\
&(c_{va}(W_{ic} + W_{egr})(T_{im,in} - T_{im}) + R_a(T_{im,in}(W_{ic} + W_{egr}) - T_{im} W_{ei})) \\
&\frac{d}{dt} p_{im} = \frac{R_a T_{im}}{V_{im}} (W_{ic} + W_{egr} - W_{ei}) + \frac{p_{im}}{T_{im}} \frac{d}{dt} T_{im}
\end{aligned} \tag{122}$$

$$\begin{aligned}
&\frac{d}{dt} T_{em} = \frac{R_e T_{em}}{p_{em} V_{em} c_{ve}} \cdot \\
&(c_{ve} W_{eo}(T_{em,in} - T_{em}) + R_e(T_{em,in} W_{eo} - T_{em}(W_t + W_{egr}))) \\
&\frac{d}{dt} p_{em} = \frac{R_e T_{em}}{V_{em}} (W_{eo} - W_t - W_{egr}) + \frac{p_{em}}{T_{em}} \frac{d}{dt} T_{em}
\end{aligned} \tag{123}$$

where the temperature $T_{im,in}$ for the flows into the intake manifold is assumed to be constant and the temperature $T_{em,in}$ for the flow into the exhaust manifold is equal to T_{em} in (24). The intercooler is assumed to be ideal, i.e.

$$W_{ic} = W_c \tag{124}$$

The differential equations for the oxygen mass fractions are the same as in Sec. 2 if (124) is applied to

$$\begin{aligned}
\frac{d}{dt} X_{Oim} &= \frac{R_a T_{im}}{p_{im} V_{im}} ((X_{Oem} - X_{Oim}) W_{egr} + (X_{Oc} - X_{Oim}) W_{ic}) \\
\frac{d}{dt} X_{Oem} &= \frac{R_e T_{em}}{p_{em} V_{em}} (X_{Oe} - X_{Oem}) W_{eo}
\end{aligned} \tag{125}$$

The values of all the tuning parameters are the same as for the 8:th order model.

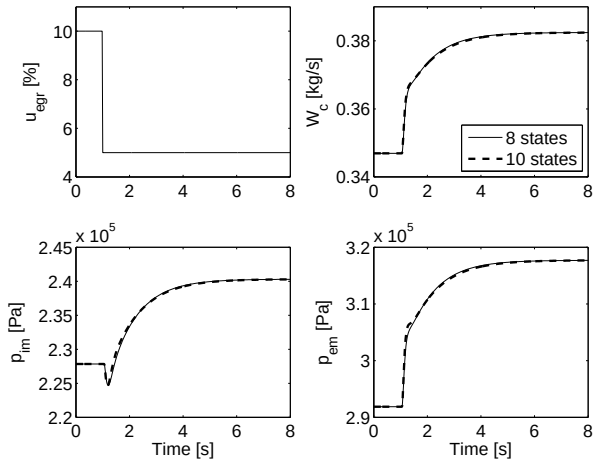

Figure 23: Comparison between 8:th and 10:th order model during a step in EGR-valve position showing that these two models have approximately the same dynamic response with a non-minimum phase behavior in p_{im}. Operating point: $u_\delta = 110$ mg/cycle, $n_e = 1500$ rpm, and $u_{vgt} = 30$ %.

9.1.2 Comparison between 8:th and 10:th order model

To investigate how the states T_{im} and T_{em} affect the system properties, step responses are compared for the 8:th and 10:th order model. Fig. 23 to Fig. 25 show that the two models have approximately the same dynamic response with approximately the same non-minimum phase behavior in p_{im} and approximately the same non-minimum phase behavior, overshoot, and sign reversal in W_c. Consequently, the temperature states only have minor effects on the system properties and therefore there are no major improvements of the model if it is extended with temperature states.

9.2 Extensions: temperature states and pressure drop over intercooler

To investigate if additional temperature states and a pressure drop over the intercooler improve the model substantially, the 10:th order model in Sec. 9.1 is extended with a control volume between the compressor and the intercooler. This control volume consists of a temperature state T_{ic} and a pressure state p_c. This leads to a 12:th order model with the states

$$x = (p_{im} \quad p_{em} \quad p_c \quad T_{im} \quad T_{em} \quad T_{ic} \quad X_{Oim} \quad X_{Oem} \quad \omega_t \quad \tilde{u}_{egr1} \quad \tilde{u}_{egr2} \quad \tilde{u}_{vgt})^T \tag{126}$$

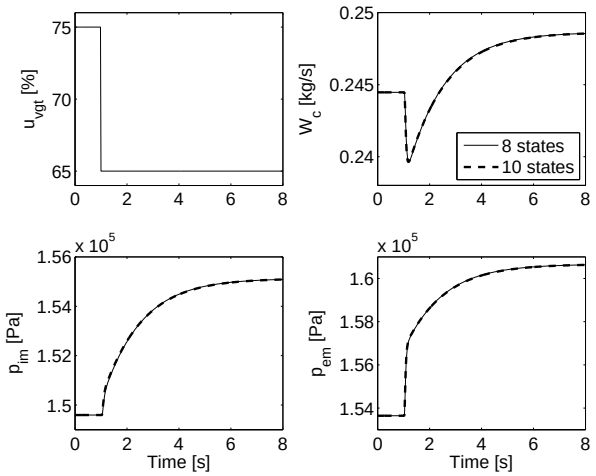

Figure 24: Comparison between 8:th and 10:th order model during a step in VGT position showing that these two models have approximately the same dynamic response with a non-minimum phase behavior in W_c. Operating point: $u_\delta = 110$ mg/cycle, $n_e = 1500$ rpm, and $u_{egr} = 80$ %.

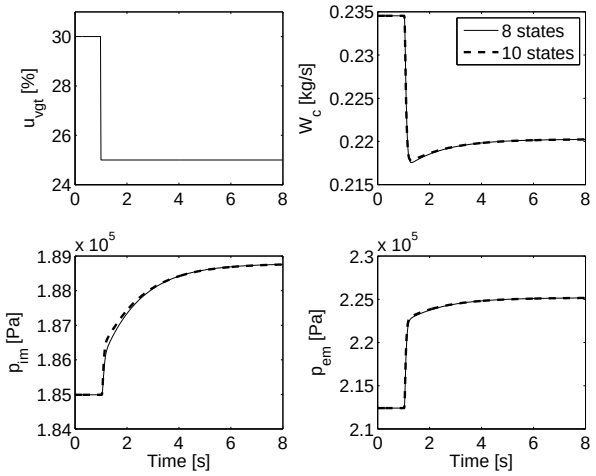

Figure 25: Comparison between 8:th and 10:th order model during a step in VGT position showing that these two models have approximately the same dynamic response with an overshoot and a sign reversal in W_c. Operating point: $u_\delta = 110$ mg/cycle, $n_e = 1500$ rpm, and $u_{egr} = 80$ %.

9.2.1 Extended model equations

The control volume before the intercooler is modeled as an adiabatic model with a temperature state T_{ic} and a pressure state p_c

$$\begin{aligned}\frac{d}{dt}T_{ic} &= \frac{R_a\,T_{ic}}{p_c\,V_{ic}\,c_{va}}\left(c_{va}\,W_c(T_c - T_{ic}) + R_a(T_c\,W_c - T_{ic}\,W_{ic})\right)\\ \frac{d}{dt}p_c &= \frac{R_a\,T_{ic}}{V_{ic}}\left(W_c - W_{ic}\right) + \frac{p_c}{T_{ic}}\frac{d}{dt}T_{ic}\end{aligned} \tag{127}$$

where V_{ic} is the volume of the control volume and it is set to a reasonable value. The flow W_{ic} through the intercooler is modeled as an incompressible flow [20, 8]

$$W_{ic} = \sqrt{\frac{p_c(p_c - p_{im})}{T_{ic}\,k_{ic}}} \tag{128}$$

Equation (128) is used instead of (124) and the pressure quotient over the compressor

$$\Pi_c = \frac{p_c}{p_{amb}} \tag{129}$$

is used instead of (58).

Tuning parameters

- k_{ic}: parameter for the model in (128)
- V_{im}: intake manifold volume
- η_{cmax}, W_{copt}, π_{copt}, c_π, a_1, a_2, and a_3: parameters for the compressor efficiency
- $c_{\Psi 2}$, $c_{\Phi 2}$, $c_{\omega\Psi 1}$, $c_{\omega\Psi 2}$, $c_{\omega\Psi 3}$, $c_{\omega\Phi 1}$, $c_{\omega\Phi 2}$, and $c_{\omega\Phi 3}$: parameters for the compressor flow

Tuning

The tuning parameter k_{ic} is determined by solving a linear least-squares problem that minimizes $(p_c - p_{im} - (p_{c,meas} - p_{im,meas}))^2$ with k_{ic} as the optimization variable. The model of $p_c - p_{im}$ is obtained by solving (128) for $p_c - p_{im}$. The variables $p_{c,meas}$ and $p_{im,meas}$ are stationary measurements.

The intake manifold volume V_{im} is re-tuned according to the method in Sec. 8.1 due to that the extended dynamics in the intercooler affects the dynamics in the intake manifold.

The tuning parameters for the compressor efficiency and the compressor flow are re-tuned using the method in Sec. 5.3 with the new definition of the pressure quotient (129).

The values of all the other tuning parameters are the same as for the 8:th order model.

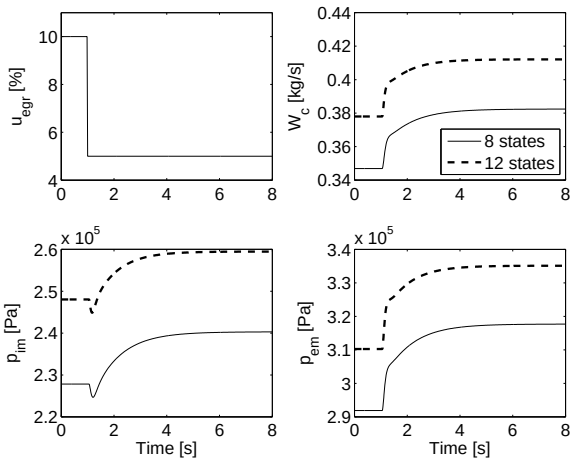

Figure 26: Comparison between 8:th and 12:th order model during a step in EGR-valve position showing that there are stationary differences. However, the dynamic behavior are approximately the same with a non-minimum phase behavior in p_{im}. Operating point: $u_\delta = 110$ mg/cycle, $n_e = 1500$ rpm, and $u_{vgt} = 30$ %.

9.2.2 Comparison between 8:th and 12:th order model

To investigate how the additional temperature states, control volume before the intercooler, and pressure drop over the intercooler affect the system properties, step responses are compared for the 8:th and 12:th order model. Fig. 26 and Fig. 27 show that there are stationary differences between the two models. However, the dynamic behavior are qualitatively the same considering the amplitudes, the time constants, and the non-minimum phase behaviors in p_{im} and W_c. In Fig. 28 there are differences in both stationary conditions and in dynamic behavior, e.g. the 12:th order model gives a non-minimum phase behavior and a positive DC-gain in p_{im} while the 8:th order model gives a response without a non-minimum phase behavior and with a negative DC-gain in p_{im}. However, by simulating the same step in an adjacent operating point, see Fig. 29, the dynamic behavior are approximately the same for the two models with a non-minimum phase behavior in p_{im} and an overshoot in p_{em}. Consequently, the two models have approximately the same dynamic behavior except that the two models change their dynamic behavior at different but adjacent operating points. Therefore, the conclusion is that temperature states, a pressure drop over the intercooler, and a control volume before the intercooler have only small effects on the dynamic behavior but the addition of the pressure drop has an effect on the stationary values.

9.2.3 Comparison between experimental data and 12:th order model

The previous section shows that there are stationary differences between the 8:th and 12:th order model. In this section, the goal is to investigate if these stationary differences improve the validation results in Sec. 8.2.

The 12:th order model is validated by calculating the mean absolute relative

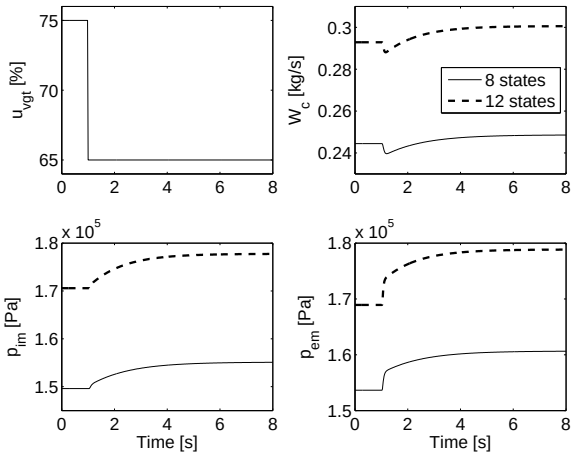

Figure 27: Comparison between 8:th and 12:th order model during a step in VGT position showing that there are stationary differences. However, the dynamic behavior are approximately the same with a non-minimum phase behavior in W_c. Operating point: $u_\delta = 110$ mg/cycle, $n_e = 1500$ rpm, and $u_{egr} = 80$ %.

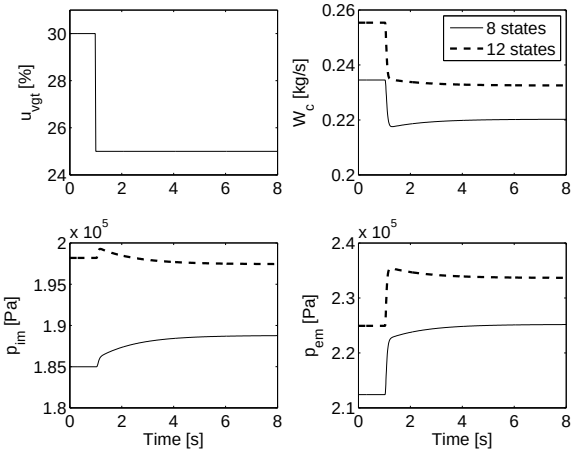

Figure 28: Comparison between 8:th and 12:th order model during a step in VGT position showing that there are differences in both stationary conditions and in dynamic behavior. Operating point: $u_\delta = 110$ mg/cycle, $n_e = 1500$ rpm, and $u_{egr} = 80$ %.

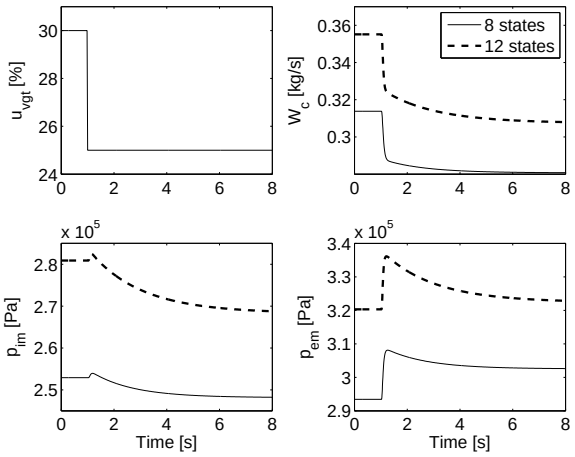

Figure 29: Comparison between 8:th and 12:th order model during a step in VGT position at an adjoining operating point compared to Fig. 28 showing that the two models have approximately the same dynamic response with a non-minimum phase behavior in p_{im} and an overshoot in p_{em}. Operating point: $u_\delta = 180$ mg/cycle, $n_e = 1500$ rpm, and $u_{egr} = 80$ %.

errors between 12:th order model and dynamic tuning or validation data, see Tab. 6. These mean absolute relative errors are calculated in the same way as for the 8:th order model in Tab. 5. Comparing these two tables, the 12:th order model gives larger mean absolute relative errors in almost all operating points and for almost all signals. There are only 6 of 37 errors that are lower. Consequently, the inclusion of temperature states, a pressure drop over the intercooler, and a control volume before the intercooler did not improve the model quality on the validation data.

Table 6: The mean absolute relative errors between diesel engine model of the 12:th order and dynamic tuning or validation data that consist of steps in VGT-position, EGR-valve, and fuel injection. These mean absolute relative errors are calculated in the same way as the mean absolute relative errors for the 8:th order model in Tab. 5. Comparing Tab. 5 and 6, the 12:th order model gives larger mean absolute relative errors for 31 of 37 errors.

	VGT-EGR steps								u_δ steps
Data set	A	B	C	D	E	F	G	H	I
Speed [rpm]	1200				1500	1900			1500
Load [%]	25	40	50	75	50	25	75	100	-
Number of steps	77	35	2	77	77	77	55	1	7
p_{im}	5.0	6.6	5.1	12.2	9.7	10.3	11.6	4.5	9.6
p_{em}	3.7	9.6	2.0	7.6	7.1	6.7	9.6	5.2	9.1
W_c	4.3	13.0	7.3	12.0	14.2	17.8	18.5	7.8	11.7
n_t	6.4	14.8	4.3	12.3	8.1	8.6	6.1	9.0	6.3
M_e	-	-	-	-	-	-	-	-	7.2

10 Conclusions

A mean value model of a diesel engine with VGT and EGR was developed and validated. The intended applications of the model are system analysis, simulation, and development of model-based control systems. The goal is to construct a model that describes the dynamics in the manifold pressures, turbocharger, EGR, and actuators with few states in order to have short simulation times. Therefore the model has only eight states: intake and exhaust manifold pressures, oxygen mass fraction in the intake and exhaust manifold, turbocharger speed, and three states describing the actuator dynamics. Many models in the literature, that approximately have the same complexity as the model proposed here, use three states for each control volume in order to describe the temperature dynamics. However, the model proposed here uses only two states for each manifold. Model extensions are investigated showing that inclusion of temperature states and pressure drop over the intercooler only has minor effects on the dynamic behavior and does not improve the model quality. Therefore, these extensions are not included in the proposed model.

Model equations and tuning methods for the parameters were described for each subsystem in the model. In order to have a low number of tuning parameters, flows and efficiencies are modeled using physical relationships and parametric models instead of look-up tables. The parameters in the static models are tuned automatically using least squares optimization and stationary measurements in 82 different operating points. The parameters in the dynamic models are tuned by adjusting these parameters manually until simulations of the complete model follow the dynamic responses in the dynamic measurements.

Static and dynamic validations of the entire model were performed using dynamic measurements, consisting of steps in fuel injection, EGR control signal, and VGT control signal. The validations show that the mean relative errors are 12.7 % or lower for all measured variables. They also show that the proposed model captures the essential system properties, i.e. a non-minimum phase behavior in the channel u_{egr} to p_{im} and a non-minimum phase behavior, an overshoot, and a sign reversal in the channel u_{vgt} to W_c.

References

[1] Ammann, M., Fekete, N., Guzzella, L., and Glattfelder, A. (2003). Model-based Control of the VGT and EGR in a Turbocharged Common-Rail Diesel Engine: Theory and Passenger Car Implementation. *SAE Technical paper 2003-01-0357*.

[2] Andersson, P. (2005). *Air Charge Estimation in Turbocharged Spark Ignition Engines*. PhD thesis, Linköpings Universitet.

[3] Björk, Å. (1996). *Numerical Methods for Least Squares Problems*. SIAM.

[4] Chevalier, A., Müeller, M., and Hendricks, E. (2000). On the validity of mean value engine models during transient operation. *SAE Technical paper 2000-01-1261*.

[5] Dixon, S. (1998). *Fluid Mechanics and Thermodynamics of Turbomachinery*. Butterworth Heinemann, Woburn, 4:th edition.

[6] Eriksson, L. (2002). Mean value models for exhaust system temperatures. *SAE 2002 Transactions, Journal of Engines, 2002-01-0374*, 111(3).

[7] Eriksson, L. (2007). Modeling and control of turbocharged SI and DI engines. *Oil & Gas Science and Technology - Rev. IFP*, 62(4):523–538.

[8] Eriksson, L., Nielsen, L., Brugård, J., Bergström, J., Pettersson, F., and Andersson, P. (2002). Modeling and simulation of a turbo charged SI engine. *Annual Reviews in Control*, 26(1):129–137.

[9] Guzzella, L. and Amstutz, A. (1998). Control of diesel engines. *IEEE Control Systems Magazine*, 18:53–71.

[10] Hendricks, E. (2001). Isothermal vs. adiabatic mean value SI engine models. In *IFAC Workshop: Advances in Automotive Control*.

[11] Heywood, J. (1988). *Internal Combustion Engine Fundamentals*. McGraw-Hill Book Co.

[12] Jankovic, M., Jankovic, M., and Kolmanovsky, I. (2000). Constructive lyapunov control design for turbocharged diesel engines. *IEEE Transactions on Control Systems Technology*.

[13] Jung, M. (2003). *Mean-Value Modelling and Robust Control of the Airpath of a Turbocharged Diesel Engine*. PhD thesis, University of Cambridge.

[14] Kolmanovsky, I., Stefanopoulou, A., Moraal, P., and van Nieuwstadt, M. (1997). Issues in modeling and control of intake flow in variable geometry turbocharged engines. In *Proceedings of* 18^{th} *IFIP Conference on System Modeling and Optimization*, Detroit.

[15] Nieuwstadt, M., Kolmanovsky, I., Moraal, P., Stefanopoulou, A., and Jankovic, M. (2000). EGR–VGT control schemes: Experimental comparison for a high-speed diesel engine. *IEEE Control Systems Magazine*.

[16] Rajamani, R. (2005). Control of a variable-geometry turbocharged and wastegated diesel engine. *Proceedings of the I MECH E Part D Journal of Automobile Engineering*.

[17] Skogtjärn, P. (2002). Modelling of the exhaust gas temperature for diesel engines. Master's thesis LiTH-ISY-EX-3379, Department of Electrical Engineering, Linköping University, Linköping, Sweden.

[18] Stefanopoulou, A., Kolmanovsky, I., and Freudenberg, J. (2000). Control of variable geometry turbocharged diesel engines for reduced emissions. *IEEE Transactions on Control Systems Technology*, 8(4).

[19] Vigild, C. (2001). *The Internal Combustion Engine Modelling, Estimation and Control Issues*. PhD thesis, Technical University of Denmark, Lyngby.

[20] Watson, N. and Janota, M. (1982). *Turbocharging the Internal Combustion Engine*. The Mechanical Press Ltd, Hong Kong.

A Notation

Table 7: Symbols used in the report

Symbol	Description	Unit
A	Area	m^2
BSR	Blade speed ratio	$-$
c_p	Spec. heat capacity, constant pressure	$J/(kg \cdot K)$
c_v	Spec. heat capacity, constant volume	$J/(kg \cdot K)$
J	Inertia	$kg \cdot m^2$
M	Torque	Nm
M_e	Engine torque	Nm
M_p	Pumping torque	Nm
n_{cyl}	Number of cylinders	$-$
n_e	Rotational engine speed	rpm
n_t	Rotational turbine speed	rpm
$(O/F)_s$	Stoichiometric oxygen-fuel ratio	$-$
p	Pressure	Pa
P	Power	W
q_{HV}	Heating value of fuel	J/kg
r_c	Compression ratio	$-$
R	Gas constant	$J/(kg \cdot K)$
R	Radius	m
T	Temperature	K
u_{egr}	EGR control signal. 100 - open, 0 - closed	%
u_{vgt}	VGT control signal. 100 - open, 0 - closed	%
u_δ	Injected amount of fuel	$mg/cycle$
V	Volume	m^3
W	Mass flow	kg/s
x_{egr}	EGR fraction	$-$
X_O	Oxygen mass fraction	$-$
γ	Specific heat capacity ratio	$-$
η	Efficiency	$-$
λ_O	Oxygen-fuel ratio	$-$
Π	Pressure quotient	$-$
ρ	Density	kg/m^3
τ	Time constant	s
Φ_c	Volumetric flow coefficient	$-$
Ψ_c	Energy transfer coefficient	$-$
ω	Rotational speed	rad/s

Table 8: Indices used in the report

Index	Description
a	air
amb	ambient
c	compressor
d	displaced
e	exhaust
egr	EGR
ei	engine cylinder in
em	exhaust manifold
eo	engine cylinder out
f	fuel
$fric$	friction
ig	indicated gross
im	intake manifold
m	mechanical
t	turbine
tc	turbocharger
vgt	VGT
vol	volumetric
δ	fuel injection

Table 9: Abbreviations used in the report

Abbreviation	Description
EGR	Exhaust gas recirculation
VGT	Variable geometry turbocharger